Transfer matrix approach to the persistent current in quantum rings: Application to hybrid normal-superconducting rings

Andrea Nava,[1] Rosa Giuliano,[1] Gabriele Campagnano,[2] and Domenico Giuliano[1]

[1]*Dipartimento di Fisica, Università della Calabria Arcavacata di Rende I-87036, Cosenza, Italy*
and I.N.F.N., Gruppo collegato di Cosenza, Arcavacata di Rende I-87036, Cosenza, Italy
[2]*CNR-SPIN, Monte S. Angelo-Via Cintia, I-80126, Napoli, Italy*
and Dipartimento di Fisica, Università di Napoli "Federico II", Monte S. Angelo-Via Cintia, I-80126 Napoli, Italy

Using the properties of the transfer matrix of one-dimensional quantum mechanical systems, we derive an exact formula for the persistent current across a quantum mechanical ring pierced by a magnetic flux Φ as a single integral of a known function of the system's parameters. Our approach provides exact results at zero temperature, which can be readily extended to a finite temperature T. We apply our technique to exactly compute the persistent current through p-wave and s-wave superconducting-normal hybrid rings, deriving full plots of the current as a function of the applied flux at various system's scales. Doing so, we recover at once a number of effects such as the crossover in the current periodicity on increasing the size of the ring and the signature of the topological phase transition in the p-wave case. In the limit of a large ring size, resorting to a systematic expansion in inverse powers of the ring length, we derive exact analytic closed-form formulas, applicable to a number of cases of physical interest.

I. INTRODUCTION

Due to the zero resistance of a superconductor, once a current is induced for instance by an applied magnetic flux Φ, in a superconducting ring, it is expected to last in principle forever. The existence of such a persistent current in superconducting rings was already predicted at the discovery of superconductivity in 1911 [1,2], and later experimentally demonstrated [3]. Remarkably, as predicted in 1983 by Büttiker, Landauer, and Imry, superconductivity is not a necessary mechanism to have persistent currents. Indeed, even a normal ring threaded by a magnetic flux can host a persistent current, provided that the temperature is low enough to suppress inelastic scattering from phonons and other electrons and that the size of the ring is short enough compared to the phase coherence length [4]. Because of the gauge invariance, both for superconducting and normal rings, the persistent current $I[\Phi]$ must be a periodic function of the magnetic flux Φ. This prediction has been eventually verified in a number of experiments [5,6]. However, while in the superconducting case the period is equal to the flux quantum appropriate for a superconductor, with current carried by Cooper pairs, $\Phi_0^* = h/(2e)$, in the normal case such a period is doubled, and equal to $\Phi_0 = h/e$.

A large amount of literature about persistent current in a normal mesoscopic ring has addressed a number of issues such as the effect of disorder in the ring with consequent possible halving in the period of the current [7,8], the role of the spin degree of freedom [9], the consequences of the electron-electron interaction, with and without impurity scattering [10], and the presence of spin-orbit interaction [11] (for a recent comprehensive review on electron transport in mesoscopic rings see, for instance, [12]). Moreover, the issue of how the current is affected by collective fluctuations in quasi-one-dimensional superconducting rings with a weak link has been considered [13], together with the possibility of using small superconducting rings, realized with pertinent

Josephson junction networks, as high-coherence quantum devices [14–16].

Recent progresses in the fabrication of nanostructures made it possible to engineer hybrid devices where superconductivity is induced by proximity effect only in a section of the ring [17] [hybrid rings (HRs)]. This enables one to explore a number of physical regimes. For instance, one may think of looking at the persistent current across the ring varying the lengths of the two regions, while keeping the length of the normal region ℓ_N shorter than the phase coherence length. In this way one may monitor the crossover between the normal mesoscopic regime, in which the length of the superconducting region ℓ_S is shorter than the superconducting coherence length ξ_0, towards the complementary Josephson-junction regime, in which $\ell_S \gg \xi_0$ [18]. Accompanied to the above crossover, one is also expected to see a crossover of the period of the persistent current, with respect to the magnetic flux, between Φ_0 (current carried by electrons) and Φ_0^* (current carried by Cooper pairs) [18,19].

A special type of HR has recently attracted great interest, in view of the possibility of designing a nonambiguous way of probing Majorana fermions (MFs) in condensed matter systems. MFs have been predicted by Kitaev to emerge as localized end modes in a spinless p-wave one-dimensional superconductor in its topological phase [20]. It has been proposed that such a system can be realized by inducing superconductivity by proximity effect in a semiconducting quantum wire with a sizable spin-orbit coupling (e.g., an InAs wire) when subject to an external magnetic field [21,22].

A zero-bias peak in a tunneling spectroscopy measurement has been claimed as an evidence for the existence of the localized MF [23], but alternative possible explanations of the experimental data of Ref. [23] have been provided, leaving still as a debated question whether a MF has been really detected, or not [24,25]. Other proposals to detect MFs have been presented, for instance, using a quantum switch made with two quantum dots coupled to MFs [26] or by means of

a local flux measurement in a topological rf-SQUID with a frustrating π junction [27] or, ultimately, of the analysis of the persistent current in metallic rings interrupted by a Coulomb blockaded topological superconducting segment [28].

When using $I[\Phi]$ as a tool to monitor the emergence of MFs, it is of the utmost importance to disentangle effects related to MF physics from "spurious" effects, which are expected to appear in nontopological phases, as well. For instance, the crossover of the period of $I[\Phi]$ vs Φ from Φ_0 to Φ_0^*, can be either attributed to MFs, or can be regarded as a simple crossover of a hybrid ring toward the mesoscopic regime, taking place when the length of the superconducting regions becomes longer than the corresponding superconducting coherence length [18,29]. Therefore, it is extremely useful to recover an exact (or pertinently approximated) formula for $I[\Phi]$, allowing us to make rigorous predictions on its dependence on the system parameters, on the length of the superconducting and nonsuperconducting regions, etc. Nevertheless, even after a number of simplifications: considering a ballistic system, using a non-self-consistent model for the superconducting region [30], or its corresponding lattice version for a s-wave [31], or for a p-wave superconductor [20], computing $I[\Phi]$ is typically still quite a challenging task. In fact, the "standard" approach to the problem consists in computing the current as

$$I[\Phi] = e\partial_\Phi \mathcal{F}[\Phi; T], \qquad (1)$$

with $\mathcal{F}[\Phi; T]$ being the system's free energy at applied flux Φ and temperature T. At $T = 0$ Eq. (1) yields

$$I[\Phi] = e\partial_\Phi E_{\mathrm{GS}}[\Phi] = e\partial_\Phi \sum_{E_n < 0} E_n, \qquad (2)$$

where the sum is taken over energies of the occupied single-quasiparticle states. To compute these energies, one has to solve the secular equation for the energy eigenvalues at nonzero Φ with periodic boundary conditions over the whole ring. In general, the resulting set of equations looks quite formidable and hard to deal with, which requires resorting to various approximations, such as retaining only the low-energy part of the spectrum [19], or employing various approximations for the single-quasiparticle energies as a function of Φ in various regions of the spectrum [18].

In this paper we present a technique that, under very general assumptions such as the ones listed above, allows for exactly expressing $I[\Phi]$ as a single integral of a pertinently constructed function of the system's parameters. At $T = 0$, our approach is based on first writing Eqs. (2) in terms of a single integral over an appropriate path in the complex energy plane, and on eventually deforming the integration path to the imaginary axis. In this respect, our method can be regarded as an adapted version of the technique developed in Refs. [32–35] to compute the dc Josephson current across an SNS junction in terms of the single-quasiparticle S matrix of the junction, which has been successfully applied to a number of cases of interest, such as the Josephson current through a chaotic Josephson junction [36], the critical supercurrent in the quantum spin-Hall effect [37], and the current across a long Josephson junction [35,38]. In fact, our method combines the idea of deforming the integration path to the imaginary axis

with the idea of using the transfer matrix, rather than the S matrix, to recover the quasiparticle scattering dynamics of the system. Indeed, while in principle the transfer matrix and the S matrix can be used on an equivalent footing to derive the transport properties of a mesoscopic system [39], the former approach comes out to be more appropriate for systems with periodic boundary conditions, such as quantum rings (see, for instance, Ref. [40] for an example of application of transfer matrix approach to the persistent current through a disordered, normal mesoscopic ring). Besides providing an exact formula allowing us to easily compute $I[\Phi]$ by numerically integrating a known function at fixed Φ, in the large-ring limit, our technique is also suitable for a systematic expansion in inverse powers of the system's length, which is the counterpart for a HR of the expansion in inverse powers of the length of a long SNS junction discussed in Ref. [35] for a single-channel system and generalized in Ref. [38] to the multichannel case. In this limit the formula for $I[\Phi]$ is greatly simplified, allowing for the derivation of analytic closed-form formulas for the current in a number of cases of interest. As an example of the effectiveness of our technique, we consistently extend the results of Refs. [28,29,41] by deriving exact plots of $I[\Phi]$ vs Φ through p-wave and s-wave superconducting-normal hybrid rings, which, by comparing the plots in the two cases with each other, allows us to highlight the features strictly related to the emergence of MFs in the p-wave case.

Remarkably, while in this paper we do not account for a number of features that can be in principle important in HRs, such as quantum phase slips [42], electronic interaction effects [10], disorder [7,8], etc., as we outline among the concluding remarks, it should not be difficult to pertinently address them within our formalism. In fact, we plan to treat some of this issues in forthcoming publications, as a natural development of this work.

The paper is organized as follows:

(1) In Sec. II we introduce the transfer matrix approach which we use to compute the persistent current.

(2) In Sec. III we introduce the lattice model Hamiltonian for a hybrid superconducting-superconducting ring, both for the p-wave and for the s-wave superconductor.

(3) In Sec. IV we compute the persistent current in some relevant reference model, such as a superconducting ring interrupted by a normal weak link, and in the case of a hybrid normal-superconducting ring. Specifically, we recover both cases as particular limit of the model introduced in Sec. III: the former one by making one of the two superconducting regions shrink to zero, the latter one by simply setting to zero the superconducting gap in one of the two regions.

(4) In Sec. V we consider the limit of large ring size in the HR both in the s-wave, and in the p-wave case. In particular, we first show how one recovers the results of Refs. [35,38] in the limit of infinite length for the superconducting region, therefore, we discuss the complementary limit of a short-superconducting and a long-normal region.

(5) In Sec. VI we outline how our results can be extended to a temperature T finite, but well below the superconducting gap. Specifically, this allows us to recover within our formalism the finite-T formula at Eq. (1).

(6) In Sec. VII we provide our main conclusions and discuss further possible developments of our work.

(7) In the Appendix we review the derivation of the subgap states in an open Kitaev chain, of finite length ℓ_S, which is functional to the discussion of the results of Sec. IV.

II. THE TRANSFER MATRIX APPROACH TO THE PERSISTENT CURRENT

Our technique to compute the persistent current through mesoscopic normal/superconducting rings is based on a combination of the approach to the Josephson current across an SNS junction based on the analytical continuation of the quasiparticle S matrix to the imaginary axis [32–35] with the transfer matrix (TM) approach to transport in mesoscopic systems [39], particularly well suited to account for periodic boundary conditions in quantum rings. The key feature of our approach is that it eventually leads to an exact, closed-form formula for the ground-state energy of the system at a given Φ and, therefore, for the persistent current across the ring. In order to illustrate its main features, in this section we review the main steps leading to our final formula for the ground-state energy in the case of a normal, mesoscopic ring. Nevertheless, as we discuss in the following, the case of a HR containing one, or more, superconducting sections is quite a straightforward generalization of the derivation we provide in this section. To treat the p-wave and the s-wave case on the same footing we choose to perform our derivation within a lattice one-dimensional model Hamiltonian, which, in the superconducting region, corresponds to Kitaev's Hamiltonian in the p-wave case [20], and to the lattice one-dimensional Hamiltonian of Ref. [31] in the s-wave case.

As an introduction to the technique presented in this article, let us consider a normal (nonsuperconducting) ring with ℓ sites as depicted in Fig. 1. We can ideally divide the ring into three regions, within the shaded region nontrivial scattering processes may happen, while in the remaining part the system is described by the asymptotic lattice Hamiltonian of the form
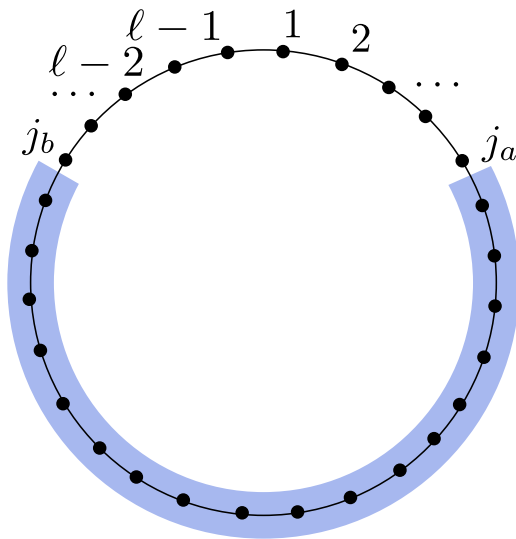

FIG. 1. An example of the ring geometry used in the article: nontrivial scattering happens in the shaded region, whereas in the remaining part one can write the wave function in terms of simple scattering states (cf. main text)

$H_{\mathrm{as}} = -J \sum_j \{c_j^\dagger c_{j+1} + c_{j+1}^\dagger c_j\} - \mu \sum_j c_j^\dagger c_j$, with c_j being the single-fermion lattice annihilation operator for spinless fermions.

Let us for the moment imagine that the ring is open at the last site ℓ and that j_1 and j_2 are limiting the region of the ring with nontrivial scattering. The wave functions at energy E in the two "asymptotic" regions for $j < j_1$ and for $j > j_2$ is

$$u_j \sim A_+^< e^{ikj} + A_-^< e^{-ikj} \quad (j < j_1),$$
$$u_j \sim A_+^> e^{ikj} + A_-^> e^{-ikj} \quad (j > j_2),$$

(3)

with

$$E = -2J \cos(k) - \mu.$$ (4)

Now, by definition the transfer matrix between sites $j_a < j_1$ and $j_b > j_2$, $\mathcal{M}[E; j_a, j_b]$, relates the solution at $j = j_a$ to the solution at $j = j_b$, that is

$$u_{j_b} = \tilde{A}_+ e^{ikj_a} + \tilde{A}_- e^{-ikj_a},$$ (5)

with

$$\begin{bmatrix} \tilde{A}_+ \\ \tilde{A}_- \end{bmatrix} = \mathcal{M}[E; j_a, j_b] \begin{bmatrix} A_+^< \\ A_-^< \end{bmatrix}.$$ (6)

Upon considering the closed geometry, we have to impose periodic boundary conditions (PBCs) on the solution in Eq. (3). Going through Eq. (5), this is accounted for by means of the secular equation

$$\mathcal{M}[E; 1, \ell] \begin{bmatrix} A_+^< \\ A_-^< \end{bmatrix} = \begin{bmatrix} A_+^< \\ A_-^< \end{bmatrix}.$$ (7)

As a result, Eq. (7) leads to the secular equation for the allowed values of the energy E:

$$\det\{\mathcal{M}[E; \ell] - \mathbf{I}\} = 0.$$ (8)

[In Eq. (8) we suppressed the dependence of $\mathcal{M}[E; j_a, j_b]$ on j_a since, as expected because of the periodic boundary conditions, it depends only on the distance between the sites, which is equal to ℓ.] Besides constituting an alternative way of presenting the eigenvalue equation for a single particle on the ring, Eq. (8) also provides an efficient way to compute the ground-state energy of the system E_{GS}, defined as the sum of all the negative (if measured with respect to the chemical potential) single-particle energy eigenvalues E_n, that is

$$E_{\mathrm{GS}} = \sum_{E_n < 0} E_n.$$ (9)

In fact, single-particle negative energy eigenvalues are just the zeros of $\det\{\mathcal{M}[E; \ell] - \mathbf{I}\}$ lying at the negative part of the real axis, if one regards $\det\{\mathcal{M}[E; \ell] - \mathbf{I}\}$ as a function of the complex variable E. To sum over all of them, we adapt the approach of Refs. [35,38], namely, we first of all note that the energy eigenvalues are the poles (with residues all equal to 1) of the function $\Psi[E; \ell]$, defined as

$$\Psi[E; \ell] = \frac{\partial_E \det\{\mathcal{M}[E; \ell] - \mathbf{I}\}}{\det\{\mathcal{M}[E; \ell] - \mathbf{I}\}} = \partial_E \ln \det\{\mathcal{M}[E; \ell] - \mathbf{I}\}.$$
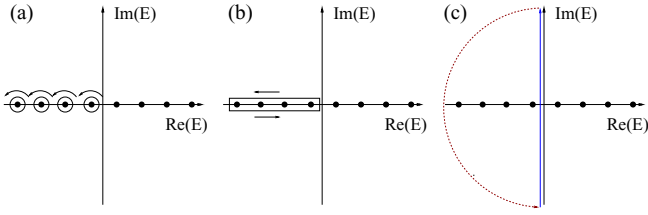
(10)

FIG. 2. Sequence of deformations in the integration path Γ eventually allowing to express $I[\Phi]$ as an integral over the imaginary axis: (a) The path Γ obtained as the union of small circles, each one surrounding one, and only one, negative (with respect to the Fermi level) energy eigenvalue. (b) The integral over Γ can be deformed to an integral over just one closed path, surrounding all the negative energy eigenvalues. (c) The integral over the red-dashed arc is assumed to be equal to 0 in the infinite-radius limit. Only the integral over the imaginary axis (to which the solid-blue line can be continuously deformed) is left.

We therefore introduce the integration path Γ depicted in Fig. 2(a) and compute E_{GS} as

$$E_{\mathrm{GS}} = \frac{1}{2\pi i} \oint_\Gamma dE \, E \, \Psi[E; \ell]$$
$$= -\frac{1}{2\pi i} \oint_\Gamma dE \, \ln \det\{\mathcal{M}[E; \ell] - \mathbf{I}\}. \quad (11)$$

On noting that $\Psi[E; \ell]$ must have no singularities outside of the real axis, we deform the integration path as illustrated in Fig. 2, so to eventually compute the integral over the imaginary axis as

$$E_{\mathrm{GS}} = -\frac{1}{2\pi} \int_{-\infty}^{\infty} d\omega \, \ln \det\{\mathcal{M}[i\omega; \ell] - \mathbf{I}\}. \quad (12)$$

Equation (12) is the heart of our article. When the ring is pierced by a magnetic field the transfer matrix $\mathcal{M}$ and hence the spectrum takes an additional dependence on the total flux Φ. We can calculate the (zero-temperature) persistent current as

$$I[\Phi] = e\partial_\Phi E_{\mathrm{GS}}[\Phi]$$
$$= -\frac{e}{2\pi} \int_{-\infty}^{\infty} d\omega \, \partial_\Phi \ln \det\{\mathcal{M}[i\omega; \ell; \Phi] - \mathbf{I}\}. \quad (13)$$

Equation (13), together with the corresponding finite-T generalization which we discuss in the following sections, is the key result of our paper and its main point of novelty: it provides an exact formula for $I[\Phi]$ which can be readily implemented, once one has derived the TM of the ring. Remarkably, while, for the sake of the presentation, in this section we relied on a normal mesoscopic ring, Eq. (13) does certainly apply equally well to the case of superconducting and/or hybrid rings, once one has constructed the appropriate TM for the system. Importantly enough, our approach allows for circumventing the main difficulty in computing the persistent current working out the single-particle energy levels, using them to compute $E_{\mathrm{GS}}[\Phi]$, and eventually employing the final result to derive the current. Besides a few, oversimplified remarkable exceptions, extracting the single-quasiparticle energy levels from the TM (or by means of an equivalent approach) is quite a difficult task to achieve, which can only be addressed either by means

of exact numerical diagonalization of the Hamiltonian (with the corresponding limitations on the system size), or within approximate methods based on truncating the full Hilbert space to a small number of low-energy (subgap) states, which are expected to carry the largest part of the current. While both these techniques are expected to suffer of strong limitations in their range of applicability, our Eq. (13) is universally applicable and, once one has constructed the TM, does not require us to go through any additional steps, besides explicitly computing the integral on the right-hand side.

Our Eq. (13) is the analog, for a superconducting ring, of the equation giving the Josephson current across an SNS junction in terms of the single-particle S matrix, analytically continued to the imaginary axis [32,34]. In this respect, it is expected by analogy to have a wide range of applicability, either as it stands, as an exact, closed form formula for $I[\Phi]$, or as a starting point to account, for instance, for the effect of disorder (in analogy to what is done in Ref. [36] for an SNS junction), or of the electronic interaction. As an example of application of our technique, in the following we derive full plots of the persistent current in hybrid superconducting-normal rings, both in the case of p-wave, and of s-wave superconductivity, which allows us to highlight the key feature that, in the former case, can be definitely attributed to the emergence of MFs at the interfaces.

As a convention on the units of measurement, in the following we shall measure the flux Φ in units of $\hbar/(2e)$, so that a period Φ_0^* corresponds to a 2π periodicity, while a period Φ_0 corresponds to a 4π periodicity.

III. MODEL HAMILTONIAN FOR A HYBRID SUPERCONDUCTING-NORMAL RING

To model a hybrid superconducting-normal ring, we resort to an effective lattice model Hamiltonian with position-dependent parameters. Using a lattice model Hamiltonian allows, on one hand, to easily introduce p-wave pairing both in real space and in momentum space, on the other hand, it provides a natural mean to regularize divergences which would arise in the continuum model when summing over the energies of the occupied levels to compute $E_{\mathrm{GS}}[\Phi]$ (and, therefore, $I[\Phi]$). To highlight special features of p-wave HRs, in the following, when possible, we systematically compare the results obtained in p-wave systems to the ones obtained in s-wave systems. Therefore, in this section we derive the transfer matrix which we shall eventually use in the following to compute the persistent current in both cases.

A. Model Hamiltonian for a p-wave nonhomogeneous superconducting ring

We here consider the system sketched in Fig. 3: a hybrid ring made of two homogeneous regions, either superconducting (p wave or s wave), or normal, each one characterized by different parameters. In the p-wave case, referring to the one-dimensional Kitaev Hamiltonian [20] for a spinless p-wave superconductor, calling 1 and 2 the two regions, we assume that the normal hopping amplitude, the pairing gap, and the chemical potential are respectively given by w_1, Δ_1, μ_1 and by w_2, Δ_2, μ_2. Moreover, we assume that regions 1 and 2
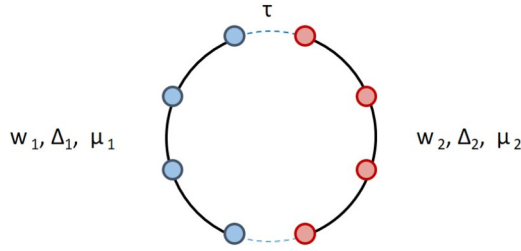
FIG. 3. Sketch of the system described by the model Hamiltonian in Eq. (14).

are coupled at their endpoints via a normal hopping term, with hopping amplitude τ. In a ring configuration, we also assume that a magnetic flux Φ pierces the ring. By means of an appropriate canonical redefinition of the lattice fermion operators, it is possible to account for the applied magnetic flux in terms of a phase factor $e^{\pm i \frac{\Phi}{4}}$, symmetrically ascribed to the two hopping terms between the two regions. As a result, we eventually present the model Hamiltonian as

$$
\begin{aligned}
H = {} & -w_1 \sum_{j=1}^{\ell_1-1} \{c_j^\dagger c_{j+1} + c_{j+1}^\dagger c_j\} - \mu_1 \sum_{j=1}^{\ell_1} c_j^\dagger c_j \\
& + \Delta_1 \sum_{j=1}^{\ell_1-1} \{c_j c_{j+1} + c_{j+1}^\dagger c_j^\dagger\} \\
& - w_2 \sum_{j=1}^{\ell_2-1} \{d_j^\dagger d_{j+1} + d_{j+1}^\dagger d_j\} - \mu_2 \sum_{j=1}^{\ell_2} d_j^\dagger d_j \\
& + \Delta_2 \sum_{j=1}^{\ell_2-1} \{d_j d_{j+1} + d_{j+1}^\dagger d_j^\dagger\} \\
& - \tau \left\{ \left[c_1^\dagger d_{\ell_2} + d_1^\dagger c_{\ell_1} \right] e^{\frac{i}{4}\Phi} + \left[d_{\ell_2}^\dagger c_1 + c_{\ell_1}^\dagger d_1 \right] e^{-\frac{i}{4}\Phi} \right\}. \quad (14)
\end{aligned}
$$

In Eq. (14) we have set the lengths of the two arms of the ring, respectively, at ℓ_1 and at ℓ_2 and used $c_j, c_j^\dagger$ to denote the lattice annihilation/creation operators at site j within region 1, and $d_j, d_j^\dagger$ to denote the lattice annihilation/creation operators at site j within region 2, with standard anticommutation relations $\{d_j, d_{j'}^\dagger\} = \{c_j, c_{j'}^\dagger\} = \delta_{j,j'}$, all the other anticommutators being equal to 0. Taken in the appropriate limit, the model Hamiltonian in Eq. (14) is suitable to describing a number of systems of physical interest, such as a p-wave superconducting ring interrupted by a weak link [41], a hybrid p-wave-normal metal ring, and a half-topological, half-nontopological superconducting ring [29]. Moreover, as we discuss in the following, taken in the limit of long-superconducting section, the superconducting-normal hybrid ring is mapped onto the effective model for a Josephson junction made with topological superconductors [43,44].

In the following, we will be mostly focusing onto the $\Delta_2 \to 0$ limit. To construct the transfer matrix, we start from the Bogoliubov–de Gennes (BdG) equations for the single-quasiparticle wave function at a given energy E. To do so, we consider a generic energy eigenmode Γ_E which, in terms of the single-fermion lattice operators on the ring, is

given by

$$
\begin{aligned}
\Gamma_E = {} & \sum_{j=1}^{\ell_1} \left\{ \left[u_j^{(1)} \right]^* c_j + \left[v_j^{(1)} \right]^* c_j^\dagger \right\} \\
& + \sum_{j=1}^{\ell_2} \left\{ \left[u_j^{(2)} \right]^* d_j + \left[v_j^{(2)} \right]^* d_j^\dagger \right\}, \quad (15)
\end{aligned}
$$

with $\left[\begin{smallmatrix} u_j^{(1)} \\ v_j^{(1)} \end{smallmatrix} \right]$ and $\left[\begin{smallmatrix} u_j^{(2)} \\ v_j^{(2)} \end{smallmatrix} \right]$ being the single-quasiparticle wave function in region 1 and in region 2. On imposing the canonical commutation relation

$$
[\Gamma_E, H] = E\Gamma_E, \quad (16)
$$

we therefore obtain the BdG equations for the wave functions. Within the homogeneous regions, these are given by

$$
\begin{aligned}
E u_j^{(1)} &= -w_1 \{ u_{j+1}^{(1)} + u_{j-1}^{(1)} \} - \mu_1 u_j^{(1)} + \Delta_1 \{ v_{j+1}^{(1)} - v_{j-1}^{(1)} \}, \\
E v_j^{(1)} &= w_1 \{ v_{j+1}^{(1)} + v_{j-1}^{(1)} \} + \mu_1 v_j^{(1)} - \Delta_1 \{ u_{j+1}^{(1)} - u_{j-1}^{(1)} \},
\end{aligned}
\quad (17)
$$

for $1 < j < \ell_1$, and

$$
\begin{aligned}
E u_j^{(2)} &= -w_2 \{ u_{j+1}^{(2)} + u_{j-1}^{(2)} \} - \mu_2 u_j^{(2)} + \Delta_2 \{ v_{j+1}^{(2)} - v_{j-1}^{(2)} \}, \\
E v_j^{(2)} &= w_2 \{ v_{j+1}^{(2)} + v_{j-1}^{(2)} \} + \mu_2 v_j^{(2)} - \Delta_2 \{ u_{j+1}^{(2)} - u_{j-1}^{(2)} \},
\end{aligned}
\quad (18)
$$

for $1 < j < \ell_2$. At the interfaces between the two regions, instead, the BdG equations yield

$$
\begin{aligned}
E u_1^{(1)} &= -w_1 u_2^{(1)} - \tau e^{-\frac{i}{4}\Phi} u_{\ell_2}^{(2)} - \mu_1 u_1^{(1)} + \Delta_1 v_2^{(1)}, \\
E v_1^{(1)} &= w_1 v_2^{(1)} + \tau e^{\frac{i}{4}\Phi} v_{\ell_2}^{(2)} + \mu_1 v_1^{(1)} - \Delta_1 u_2^{(1)}, \\
E u_{\ell_2}^{(2)} &= -w_2 u_{\ell_2-1}^{(2)} - \tau e^{\frac{i}{4}\Phi} u_1^{(1)} - \mu_2 u_{\ell_2}^{(2)} - \Delta_2 v_{\ell_2-1}^{(2)}, \\
E v_{\ell_2}^{(2)} &= w_2 v_{\ell_2-1}^{(2)} + \tau e^{-\frac{i}{4}\Phi} v_1^{(1)} + \mu_2 v_{\ell_2}^{(2)} + \Delta_2 u_{\ell_2-1}^{(2)}, \\
E u_1^{(2)} &= -w_2 u_2^{(2)} - \tau e^{-\frac{i}{4}\Phi} u_{\ell_1}^{(1)} - \mu_2 u_1^{(2)} + \Delta_2 v_2^{(2)}, \\
E v_1^{(2)} &= w_2 v_2^{(2)} + \tau e^{\frac{i}{4}\Phi} v_{\ell_1}^{(1)} + \mu_2 v_1^{(2)} - \Delta_2 u_2^{(2)}, \\
E u_{\ell_1}^{(1)} &= -w_1 u_{\ell_1-1}^{(1)} - \tau e^{\frac{i}{4}\Phi} u_1^{(2)} - \mu_1 u_{\ell_1}^{(1)} - \Delta_1 v_{\ell_1-1}^{(1)}, \\
E v_{\ell_1}^{(1)} &= w_1 v_{\ell_1-1}^{(1)} + \tau e^{-\frac{i}{4}\Phi} v_1^{(2)} + \mu_1 v_{\ell_1}^{(1)} + \Delta_1 u_{\ell_1-1}^{(1)}. \quad (19)
\end{aligned}
$$

According to Eqs. (17) and (18), within the homogeneous regions, we write the wave functions as superpositions of the solutions of the homogeneous BdG equations, that is, we set

$$
\begin{bmatrix} u_j \\ v_j \end{bmatrix} = \begin{bmatrix} u^{(1)} \\ v^{(1)} \end{bmatrix} e^{ik_1 j} \quad (20)
$$

in region 1, with $1 \leqslant j \leqslant \ell_1$, and

$$
\begin{bmatrix} u_j \\ v_j \end{bmatrix} = \begin{bmatrix} u^{(2)} \\ v^{(2)} \end{bmatrix} e^{ik_2 j} \quad (21)
$$

in region 2, with $1 \leqslant j \leqslant \ell_2$. At a given energy E, the amplitudes $\left[\begin{smallmatrix} u^{(a)} \\ v^{(a)} \end{smallmatrix} \right]$ ($a = 1,2$) are determined by solving the equations

$$
\begin{aligned}
0 &= \{ E + 2w_a \cos(k_a) + \mu_a \} u^{(a)} - 2i\Delta_a \sin(k_a) v^{(a)}, \\
0 &= 2i\Delta_a \sin(k_a) u^{(a)} + \{ E - 2w_a \cos(k_a) - \mu_a \} v^{(a)},
\end{aligned}
\quad (22)
$$

with k_1, k_2 determined by the dispersion relations

$$
\begin{aligned}
E^2 &= [2w_1\cos(k_1) + \mu_1]^2 + 4\Delta_1^2\sin^2(k_1) \\
&= [2w_2\cos(k_2) + \mu_2]^2 + 4\Delta_2^2\sin^2(k_2).
\end{aligned}
\tag{23}
$$

Solving Eq. (23) at a given energy, we define the particlelike momenta $k_p^{(a)}$ and the holelike momenta $k_h^{(a)}$ as

$$
\cos\left(k_p^{(a)}\right) = -\frac{w_a\mu_a}{2(w_a^2 - \Delta_a^2)} - \frac{1}{2}\sqrt{\frac{E^2 - \left[\Delta_w^{(a)}\right]^2}{w_a^2 - \Delta_a^2}},
$$

$$
\cos\left(k_h^{(a)}\right) = -\frac{w_a\mu_a}{2(w_a^2 - \Delta_a^2)} + \frac{1}{2}\sqrt{\frac{E^2 - \left[\Delta_w^{(a)}\right]^2}{w_a^2 - \Delta_a^2}},
\tag{24}
$$

with

$$
\Delta_w^{(a)} = \Delta_a\sqrt{4 - \frac{\mu_a^2}{w_a^2 - \Delta_a^2}}.
\tag{25}
$$

[Note that Eqs. (24) do in principle hold also for $|E| < \Delta_w^{(a)}$.] At given $k_p^{(a)}, k_h^{(a)}$, one determines the wave functions $(u_p^{(a)}, v_p^{(a)})$ and $(u_h^{(a)}, v_h^{(a)})$, defined as solutions of Eqs. (22) with k_a respectively equal to k_p and k_h. Taking the most general linear combinations of wave functions at the same energy, one finds that a generic wave function at energy E within region a (=1,2) takes the form

$$
\begin{aligned}
\begin{bmatrix} u_j^{(a)} \\ v_j^{(a)} \end{bmatrix} &= A_{(p,+)}^{(a)}\begin{bmatrix} u_p^{(a)} \\ v_p^{(a)} \end{bmatrix}e^{ik_p^{(a)}j} + A_{(p,-)}^{(a)}\begin{bmatrix} u_p^{(a)} \\ -v_p^{(a)} \end{bmatrix}e^{-ik_p^{(a)}j} \\
&\quad + A_{(h,+)}^{(a)}\begin{bmatrix} u_h^{(a)} \\ -v_h^{(a)} \end{bmatrix}e^{-ik_h^{(a)}j} + A_{(h,-)}^{(a)}\begin{bmatrix} u_h^{(a)} \\ v_h^{(a)} \end{bmatrix}e^{ik_h^{(a)}j}.
\end{aligned}
\tag{26}
$$

The transfer matrix is fully determined once one recovers the relations between the amplitudes $A_{(p,+)}^{(a)}, A_{(p,-)}^{(a)}$, $A_{(h,+)}^{(a)}, A_{(h,-)}^{(a)}$ in the two regions. These are determined by the interface conditions obtained from Eqs. (19). In a compact notation, these are given by

$$
\begin{aligned}
&\Sigma_a[\Phi][\Upsilon^{(a)}(E)]\begin{bmatrix} A_{(p,+)}^{(a)} \\ A_{(p,-)}^{(a)} \\ A_{(h,+)}^{(a)} \\ A_{(h,-)}^{(a)} \end{bmatrix} \\
&= \Omega_b[\Phi][\Upsilon^{(b)}(E)]\mathbf{T}_b(E;\ell_b)\begin{bmatrix} A_{(p,+)}^{(b)} \\ A_{(p,-)}^{(b)} \\ A_{(h,+)}^{(b)} \\ A_{(h,-)}^{(b)} \end{bmatrix},
\end{aligned}
\tag{27}
$$

with $b = 2(1)$ if $a = 1(2)$, and the matrix $\Sigma_a[\Phi]$ defined as

$$
\Sigma_a[\Phi] = \begin{bmatrix} \tau e^{\frac{i}{4}\Phi} & 0 & 0 & 0 \\ 0 & \tau e^{-\frac{i}{4}\Phi} & 0 & 0 \\ 0 & 0 & w_a & \Delta_a \\ 0 & 0 & \Delta_a & w_a \end{bmatrix},
\tag{28}
$$

the matrix $[\Upsilon^{(a)}(E)]$ defined as

$$
[\Upsilon^{(a)}(E)] = \begin{bmatrix} e^{ik_p^{(a)}}u_p^{(a)} & e^{-ik_p^{(a)}}u_p^{(a)} & e^{-ik_h^{(a)}}u_h^{(a)} & e^{ik_h^{(a)}}u_h^{(a)} \\ e^{ik_p^{(a)}}v_p^{(a)} & -e^{-ik_p^{(a)}}v_p^{(a)} & -e^{-ik_h^{(a)}}v_h^{(a)} & e^{ik_h^{(a)}}v_h^{(a)} \\ u_p^{(a)} & u_p^{(a)} & u_h^{(a)} & u_h^{(a)} \\ v_p^{(a)} & -v_p^{(a)} & -v_h^{(a)} & v_h^{(a)} \end{bmatrix},
\tag{29}
$$

the matrix $\Omega_a[\Phi]$ given by

$$
\Omega_a[\Phi] = \begin{bmatrix} w_a & -\Delta_a & 0 & 0 \\ -\Delta_a & w_a & 0 & 0 \\ 0 & 0 & \tau e^{-\frac{i}{4}\Phi} & 0 \\ 0 & 0 & 0 & \tau e^{\frac{i}{4}\Phi} \end{bmatrix},
\tag{30}
$$

and, finally, the transfer matrix for a homogeneous region of length ℓ being given by

$$
\mathbf{T}_a(E;\ell) = \begin{bmatrix} e^{ik_p^{(a)}\ell} & 0 & 0 & 0 \\ 0 & e^{-ik_p^{(a)}\ell} & 0 & 0 \\ 0 & 0 & e^{-ik_h^{(a)}\ell} & 0 \\ 0 & 0 & 0 & e^{ik_h^{(a)}\ell} \end{bmatrix}.
\tag{31}
$$

As a result, the transfer matrix for the full ring takes the form

$$
\begin{aligned}
\mathcal{M}_{p\text{-wave}}[E;\Phi;\ell_1;\ell_2] &= [\Upsilon^{(2)}(E)]^{-1}\Sigma_2^{-1}[\Phi]\Omega_1[\Phi][\Upsilon^{(1)}(E)] \\
&\quad \times \mathbf{T}_1(E;\ell_1)[\Upsilon^{(1)}(E)]^{-1}\Sigma_1^{-1}[\Phi] \\
&\quad \times \Omega_2[\Phi][\Upsilon^{(2)}(E)]\mathbf{T}_2(E;\ell_2).
\end{aligned}
\tag{32}
$$

Equation (32) is the key ingredient we need to compute the persistent current in the various regimes of interest. As stated above, we now derive the analog of Eq. (32) in the case of a ring made of s-wave superconducting regions.

B. Model Hamiltonian for an s-wave nonhomogeneous superconducting ring

In the case of a system made of two s-wave superconducting regions with parameters respectively given by w_1, Δ_1, μ_1 and by w_2, Δ_2, μ_2, and connected to each other with hopping amplitude τ, the corresponding (spinful) Hamiltonian is given by

$$
\begin{aligned}
H &= -w_1\sum_\sigma\sum_{j=1}^{\ell_1-1}\{c_{j,\sigma}^\dagger c_{j+1,\sigma} + c_{j+1,\sigma}^\dagger c_{j,\sigma}\} \\
&\quad -\mu_1\sum_\sigma\sum_{j=1}^{\ell_1}c_{j,\sigma}^\dagger c_{j,\sigma} + \Delta_1\sum_{j=1}^{\ell_1}\{c_{j,\uparrow}c_{j,\downarrow} + c_{j,\downarrow}^\dagger c_{j,\uparrow}^\dagger\} \\
&\quad -w_2\sum_\sigma\sum_{j=1}^{\ell_2-1}\{d_{j,\sigma}^\dagger d_{j+1,\sigma} + d_{j+1,\sigma}^\dagger d_{j,\sigma}\} \\
&\quad -\mu_2\sum_\sigma\sum_{j=1}^{\ell_2}d_{j,\sigma}^\dagger d_{j,\sigma} + \Delta_2\sum_{j=1}^{\ell_2}\{d_{j,\uparrow}d_{j,\downarrow} + d_{j,\downarrow}^\dagger d_{j,\uparrow}^\dagger\} \\
&\quad -\sum_\sigma\tau\{[c_{1,\sigma}^\dagger d_{\ell_2,\sigma} + d_{1,\sigma}^\dagger c_{\ell_1,\sigma}]e^{\frac{i}{4}\Phi} \\
&\quad + [d_{\ell_2,\sigma}^\dagger c_{1,\sigma} + c_{\ell_1,\sigma}^\dagger d_{1,\sigma}]e^{-\frac{i}{4}\Phi}\}.
\end{aligned}
\tag{33}
$$

Going through the same steps as in the p-wave case, we eventually find that the transfer matrix of the ring is now given by

$$\mathcal{M}_{s\text{-wave}}[E;\Phi;\ell_1;\ell_2] = [\tilde{\Upsilon}^{(2)}(E)]^{-1}\tilde{\Sigma}_2^{-1}[\Phi]\tilde{\Omega}_1[\Phi][\tilde{\Upsilon}^{(1)}(E)]$$
$$\times \mathbf{T}_1(E;\ell_1)[\tilde{\Upsilon}^{(1)}(E)]^{-1}\tilde{\Sigma}_1^{-1}[\Phi]$$
$$\times \tilde{\Omega}_2[\Phi][\tilde{\Upsilon}^{(2)}(E)]\mathbf{T}_2(E;\ell_2). \quad (34)$$

The $\tilde{\Sigma}_a[\Phi], \tilde{\Omega}_a[\Phi]$ matrices in Eq. (34) are simply obtained by setting Δ_a to 0 respectively in Eqs. (28) and (30). The matrix $[\tilde{\Upsilon}^{(a)}(E)]$ is given by

$$[\tilde{\Upsilon}^{(a)}(E)] = \begin{bmatrix} e^{ik_p^{(a)}}u_p^{(a)} & e^{-ik_p^{(a)}}u_p^{(a)} & e^{-ik_h^{(a)}}u_h^{(a)} & e^{ik_h^{(a)}}u_h^{(a)} \\ e^{ik_p^{(a)}}v_p^{(a)} & e^{-ik_p^{(a)}}v_p^{(a)} & e^{-ik_h^{(a)}}v_h^{(a)} & e^{ik_h^{(a)}}v_h^{(a)} \\ u_p^{(a)} & u_p^{(a)} & u_h^{(a)} & u_h^{(a)} \\ v_p^{(a)} & v_p^{(a)} & v_h^{(a)} & v_h^{(a)} \end{bmatrix},$$

$$(35)$$

with $u^{(a)}, v^{(a)}$ determined as nontrivial solutions of the algebraic system

$$0 = \{E + 2w_a\cos(k_a) + \mu_a\}u^{(a)} - \Delta_a v^{(a)},$$
$$0 = -\Delta_a u^{(a)} + \{E - 2w_a\cos(k_a) - \mu_a\}v^{(a)}, \quad (36)$$

for k_1, k_2 solving the secular equation

$$E^2 = [2w_1\cos(k_1) + \mu_1]^2 + \Delta_1^2$$
$$= [2w_2\cos(k_2) + \mu_2]^2 + \Delta_2^2, \quad (37)$$

and $k_p^{(a)}, k_h^{(a)}$ defined by

$$\cos[k_p^{(a)}] = -\frac{\mu_a}{2w_a} - \sqrt{\frac{E^2 - \Delta_a^2}{4w_a^2}},$$

$$\cos[k_h^{(a)}] = -\frac{\mu_a}{2w_a} + \sqrt{\frac{E^2 - \Delta_a^2}{4w_a^2}}. \quad (38)$$

Besides the differences in the form of the matrices appearing in Eqs. (32) and (34), an important point to stress is that both matrices are block factorizable, with the factorization corresponding to the possibility of regarding the system as a sequence of homogeneous regions separated by interfaces. Indeed, the TM for a one-dimensional system comes out to be simply the ordered product of the matrices corresponding to the homogeneous regions and of the ones corresponding to the interfaces, taken in the appropriate sequence. From this respect, the matrices corresponding to each homogeneous region and to each interface are sort of "building blocks" of the global transfer matrix (see Fig. 4 for a sketch of the factorizability of the matrix).

IV. CALCULATION OF THE PERSISTENT CURRENT

In this section we compute the persistent current in a number of cases of interest. To highlight the feature related to the emergence of MFs at the SN interfaces, it is worth comparing the results obtained in p-wave systems with the ones obtained in s-wave systems. Therefore, in the following we perform the calculation in both cases, by using Eq. (13), with the transfer
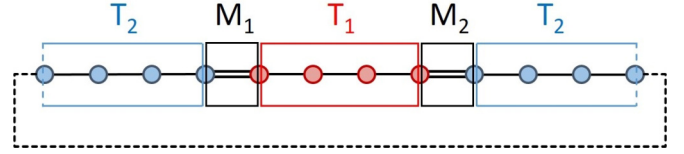

FIG. 4. Graphical representation of the factorizability of the transfer matrix: for the specific system depicted in the figure, the transfer matrix is given by $\mathcal{M} = \mathbf{T}_2 M_1 \mathbf{T}_1 M_2 \mathbf{T}_2$ (from right to left).

matrix computed according to Eq. (32) (p-wave case), or to Eq. (34) (s-wave case). To keep in touch with the results of Ref. [29], we begin with the calculation of the current in the case of a superconducting ring interrupted by a weak link though, at variance with the discussion of Ref. [29], we will not assume fermion parity conservation. As stated above, for comparison, we also compute the current in the case of a ring made with an s-wave superconductor.

A. Persistent current across a superconducting ring interrupted by a weak link

A p-wave superconducting ring interrupted by a weak link can be physically realized at a semiconducting quantum wire with a sizable spin-orbit coupling (e.g., an InAs wire) deposited onto a bulk superconducting ring pierced by a magnetic flux Φ. The combined effect of spin-orbit coupling, Zeeman spin splitting, and proximity-induced superconductivity from the bulk superconductor underneath has been shown to make the wire effectively behave as a one-dimensional p-wave superconductor [21,22]. As for what concerns a concrete proposal of an experimental realization of the p-wave HR, we refer to Refs. [28,29]. Specifically, we assume that the weak link is actually realized as a physical interruption of the superconducting ring with a tiny insulating layer, which cuts the current within the superconductor, thus allowing the persistent current to only flow across the semiconducting nanowire. In fact, among other advantages, this geometry allows for recovering as only detectable current the one flowing through the semiconducting wire, which is what we are eventually interested in. An important point to stress is that it is typically difficult to keep the ring perfectly isolated from the substrate, so to avoid fermion parity nonconserving relaxation processes [29–45]. Moreover, in order for the grand-canonical-like description of our system we employ here to be reliable, one has to think of a ring in contact with a substrate, working as an electronic reservoir. Therefore, we should not expect fermion parity to be preserved here. For this reason, though one might in principle account for fermion parity conservation by implementing some pertinent adapted version of the approach presented in Ref. [37], throughout all our paper we assume fermion parity not to be conserved which, nevertheless, does not affect the possibility of probing emergent MFs by means of an appropriate persistent current measurement.

In Fig. 5 we provide a sketch of the system we are considering here, that is, a homogeneous ring interrupted by a weak link. The corresponding model Hamiltonian can be recovered from Eq. (14) in the p-wave case and from Eq. (33) in the s-wave case, by setting to zero the length of one of the
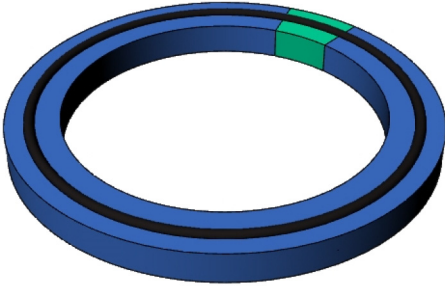
FIG. 5. Sketch of the superconducting ring interrupted by a weak link as introduced and discussed in Ref. [29]. A semiconducting ring (depicted as a solid black line) is deposited on top of a bulk superconducting ring, interrupted by a tiny insulating layer (light blue sector). The superconductor induces superconductivity within the semiconducting wire by proximity effect. All the current circulating across the system is due to tunneling effect within the semiconducting wire.

two regions. In the former case, it is given by

$$
H_{p-w} = -w \sum_{j=1}^{\ell-1} \{c_j^\dagger c_{j+1} + c_{j+1}^\dagger c_j\} - \mu \sum_{j=1}^{\ell} c_j^\dagger c_j
$$
$$
+ \Delta \sum_{j=1}^{\ell-1} \{c_j c_{j+1} + c_{j+1}^\dagger c_j^\dagger\}
$$
$$
- \tau \{c_1^\dagger c_\ell e^{\frac{i}{2}\Phi} + c_\ell^\dagger c_1 e^{-\frac{i}{2}\Phi}\}, \qquad (39)
$$

while in the latter case it can be presented as

$$
H_{s-w} = -w \sum_\sigma \sum_{j=1}^{\ell-1} \{c_{j,\sigma}^\dagger c_{j+1,\sigma} + c_{j+1,\sigma}^\dagger c_{j,\sigma}\}
$$
$$
- \mu \sum_\sigma \sum_{j=1}^{\ell_1} c_{j,\sigma}^\dagger c_{j,\sigma} + \Delta \sum_{j=1}^{\ell} \{c_{j,\uparrow} c_{j,\downarrow} + c_{j,\downarrow}^\dagger c_{j,\uparrow}^\dagger\}
$$
$$
- \sum_\sigma \tau \{c_{1,\sigma}^\dagger c_{\ell,\sigma} e^{\frac{i}{2}\Phi} + c_{\ell,\sigma}^\dagger c_{1,\sigma} e^{-\frac{i}{2}\Phi}\}. \qquad (40)
$$

Let us note that, in this case, the flux is fully "loaded" on the single hopping term. The transfer matrix derived from Eqs. (39) and (40) can therefore be simply expressed in terms of the ones we provide in Sec. III B by simply setting one of the two lengths (say ℓ_2) to 0. We therefore obtain

$$
\mathcal{M}_{p-w}[E;\ell;\Phi] = [\Upsilon(E)]^{-1} \Sigma^{-1}[2\Phi] \Omega[2\Phi][\Upsilon(E)] \mathbf{T}[E;\ell],
$$
$$(41)$$

and, similarly

$$
\mathcal{M}_{s-w}[E;\ell;\Phi] = [\tilde\Upsilon(E)]^{-1} \tilde\Sigma^{-1}[2\Phi] \tilde\Omega[2\Phi][\tilde\Upsilon(E)] \mathbf{T}[E;\ell].
$$
$$(42)$$

To compute the current, let us start with the ring described by the TM in Eq. (41). In Fig. 6 we plot $I[\Phi]$ vs Φ for the values of the parameters reported in the caption, particularly for a chemical potential $\mu = 0$. At zero chemical potential, the p-wave superconductor lies well within the topological region, with two MFs γ_L, γ_R localized at its endpoints. This
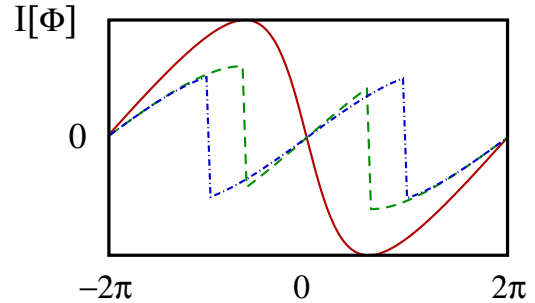

FIG. 6. Plot of the persistent current $I[\Phi]$ vs Φ (in units of Φ_0) for the p-wave mesoscopic ring with a weak link described by Eq. (39). The parameters are chosen so that $\mu = 0$, $\Delta = 0.2$, and $\tau = 0.5$ (in units of w), $\ell = 4$ (full red curve), $\ell = 8$ (dashed green curve), $\ell = 40$ (dot-dashed blue curve). The estimated Majorana hybridization length in this case is $\ell_M \approx 5$.

allows us to provide a simple interpretation of the curves we draw in Fig. 6 at different values of the length ℓ of the superconductor. The key parameter here is the "hybridization length" ℓ_M between γ_L and γ_R, which we estimate according to the derivation of the Appendix. At $\mu = 0$ and for the values of the parameters we used, from Eq. (A13) we obtain $\ell_M \sim 5$. Therefore, when considering the largest ring ($\ell = 40$), we may safely neglect the overlap between γ_L and γ_R across the superconducting region and accordingly describe the low-energy excitations of the system by approximating the fermion operators in the tunneling term of the total Hamiltonian [second row of Eq. (39)] by means of the truncated mode expansion in Eq. (A19). As a result, we obtain the effective low-energy Hamiltonian $H_{p;\mathrm{Eff}}$ for the ring, given by

$$
H_{p;\mathrm{Eff}} \approx -\epsilon_0 \cos\left(\frac{\Phi}{2}\right) \{2\Gamma^\dagger \Gamma - 1\}, \qquad (43)
$$

with $\epsilon_0 \propto \tau$ and the Dirac fermion operator Γ related to γ_L, γ_R by means of Eqs. (A22). We now use Eq. (43) as a main reference to discuss the behavior of the current for large ℓ. In fact, while one should, in principle, consider the contributions arising from all the populated single-quasiparticle states at any energy (which is exactly done in the calculation we performed based on our TM approach), based upon arguments similar to the ones provided in Refs. [35,38], in the large-ℓ limit we expect that the result for $I[\Phi]$ can be safely recovered by taking into account only low-energy states of the system. Now, for $-\pi < \Phi < \pi$, Eq. (43) tells us that the ground state has the Γ level populated. As Φ crosses π, there is a crossing between the filled- and the empty-Γ state which, in the absence of constraints on fermion parity conservation, makes the system "jump" from the populated to the empty Γ-fermion state, with the corresponding jump in the current evidenced at $\Phi = \pi$ in the blue curve of Fig. 6, corresponding to $\ell = 40$. By symmetry $\Phi \to -\Phi$, an analogous jump is observed at $\Phi = -\pi$. The total current is periodic, with period equal to 2π, due to the sequential level crossings at $\Phi = 2\pi k + \pi$, with integer k [22].

At variance, as $\ell = 4$, the hybridization between the MFs across the topological superconductor is no longer negligible. As a result, at low energy the system is described by an effective Hamiltonian such as the one in Eq. (A24), with
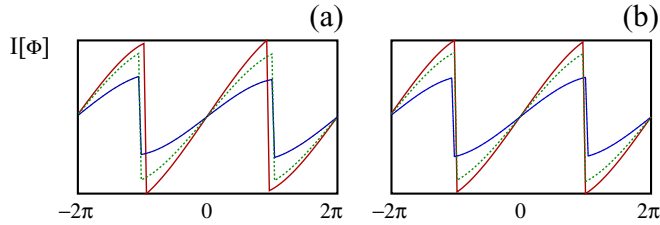
FIG. 7. Plot of the persistent current $I[\Phi]$ vs Φ (in units of Φ_0) for the p-wave mesoscopic ring with a weak link described by Eq. (39). The parameters are chosen so that $\Delta = 0.2$ and $\tau = 0.5$ (in units of w). The curves are plotted for various values of μ at fixed ℓ. Specifically (a) $\ell = 16$, $\mu = 0.0$ (full red curve), $\mu = 0.9$ (dashed green curve), $\mu = 1.5$ (dot-dashed blue curve) and (b) $\ell = 40$, $\mu = 0.0$ (full red curve), $\mu = 0.9$ (dashed green curve), $\mu = 1.5$ (dot-dashed blue curve).

FIG. 8. Plot of the persistent current $I[\Phi]$ vs Φ (in units of Φ_0) for the s-wave mesoscopic ring with a weak link described by Eq. (40). The parameters are chosen so that $\Delta = 0.2$ and $\tau = 0.5$ (in units of w). The curves are plotted for various values of ℓ at $\mu = 0$. Specifically $\ell = 4$ (full red curve), $\ell = 16$ (dashed green curve), $\ell = 40$ (dot-dashed blue curve). The crossover from a 4π periodicity for $\ell < \xi_0 \sim 10$ (see text) to a 2π periodicity for $\ell > \xi_0$ is apparent.

a modulation with Φ of the energy splitting between the empty and the filled state, which never closes (avoided level crossing). In this case, the persistent current is only supported by Cooper pair tunneling across the weak link, which restores a 4π periodicity in Φ [22]. Again, this is consistent with our plot in Fig. 6 for $\ell = 4$, with the intermediate case $\ell = 8$ lying in between the two "asymptotic" cases. As a further check, we report in Fig. 7 the plots of $I[\Phi]$ generated by keeping $w = 1, \Delta = 0.2, \tau = 0.5$ and varying μ, with $\ell = 16$ [Fig. 7(a)] and $\ell = 40$ [Fig. 7(b)] (note that $\ell_M \sim 5$, as estimated above). From the plots we draw for $\mu = 0.0, 0.9, 1.5$, we see that, increasing μ toward the critical value $\mu = 2$ at which the topological phase transition takes place [20], effectively corresponds to increasing ℓ_M. This is expected from the results of the Appendix, where we show that the hybridization between γ_L and γ_R scales as $e^{-\ell/\ell_M}$. Thus, again our results appear to be consistent with the low-energy dynamics of our system as inferred from the Appendix and from the discussion reported in Ref. [22].

By contrast, we now discuss the current across an s-wave ring. Despite the lack of low-energy MFs in such a system, the crossover in the periodicity of $I[\Phi]$ from 4π to 2π is known to take place as the length ℓ_S of the superconducting region crosses over from values lower than the coherence length ξ_0 to values higher than ξ_0 [19]. Such a crossover corresponds to a crossover in the "physical nature" of $I[\Phi]$: from a 4π-persistent current in a mesoscopic, effectively normal, system to a 2π-periodic current, analogous to the Josephson supercurrent in an SNS junction [18,19]. In Fig. 8 we plot the exact results for $I[\Phi]$ obtained using our TM approach for the system parameters $w = 1, \Delta = 0.2, \mu = 0, \tau = 0.5$ and for various values of ℓ. In our specific case, having as model Hamiltonian the one in Eq. (40), as we are setting to 1 the lattice step, an acceptable estimate for ξ_0 is $\xi_0 \sim 2w/\Delta$. For the numerical values of the parameters we chose to generate Fig. 8, this implies $\xi_0 \sim 10$. Such an estimate is definitely consistent with our results: on increasing ℓ from $\ell = 4$ to $\ell = 40$, we ultimately see a crossover in the periodicity of $I[\Phi]$ definitely similar to the one we found for the p-wave superconducting ring with a weak link, though without the jumps in the current due to the Γ-fermion level crossings. To conclude this section, let us stress once more that our technique does provide us
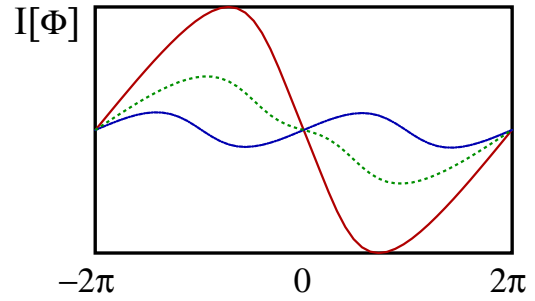
with the exact result for $I[\Phi]$ at a generic value of the system parameters, whether the superconductor is p wave, or s wave, etc. To recover the final result one just needs to construct the appropriate TM and to numerically compute a single integral for various values of Φ. Using the standard approach, based on the solution of the secular equations for the allowed values of the momenta at fixed Φ, and eventually taking the derivative with respect to Φ to obtain the current is, in general, much less straightforward and, typically, exact results cannot be provided and different approximations must be implemented to attack different regimes such as the short-ring, or the long-ring limit (see Ref. [18] for a careful and valuable discussion about this point). At variance, as we are showing here, our approach applies to any specific case, with potentially no limitations at all. It allows us to recover the full plots of the persistent current at various system scales, which we show in this section and in the following one: an original result that complements and extends the analysis of Ref. [29], where the analysis of the current was performed by just considering how the relative weight of the first two harmonics (in Φ) varies, as a function of the system parameters. In the following, to discuss a further application of our technique, we consider a hybrid ring, made by a p-wave superconducting segment of length ℓ_S and a normal segment of length ℓ_N: this can be regarded as a generalization of the ring with a weak link which, as we are going to discuss, opens the way to a number of interesting physical effects.

B. Persistent current across a hybrid N-S ring

In this section we discuss the persistent current across a hybrid ring, composed of a superconducting segment of length ℓ_S and of a normal segment of length ℓ_N. Such a system can be regarded as a generalization of the ring interrupted by a weak link discussed in Ref. [29], in which one induced superconductivity by proximity only in a part of the ring, leaving a finite normal region of length ℓ_N. In Fig. 9 we provide a sketch of the system we discuss here. Again, for comparison, we consider both cases of a p-wave and of an s-wave superconducting region. The corresponding model Hamiltonian can then be obtained from H in Eq. (14) by
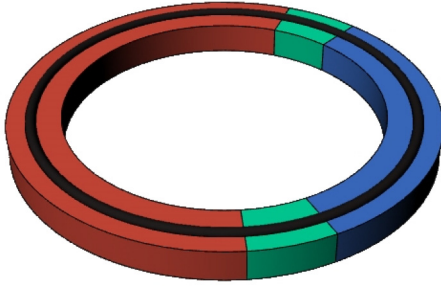
FIG. 9. Sketch of the hybrid N-S ring with the two regions (red and blue, respectively) separated by two weak links. A possible practical realization of such a system is the same as discussed before for the superconducting ring interrupted by a weak link.

setting $\ell_1 \to \ell_S$, $\ell_2 \to \ell_N$, $\Delta_1 \to \Delta$, $\Delta_2 = 0$ and from H in Eq. (33), taken in the same limit. To spell out the behavior of $I[\Phi]$ in the various regimes of interest, let us first focus onto the p-wave case. Specifically, we compute $I[\Phi]$ at given τ and Δ for $w_1 = w_2 \equiv w$ and for various values of $\ell_S = \ell_N \equiv \ell$. To further simplify the calculation we restrict ourselves to the particle-hole symmetric case $\mu = 0$.

In Fig. 10(a) we plot $I[\Phi]$ vs Φ for $\ell = 4, 16, 40$, with the values for the system's parameters chosen as in the caption. The behavior of $I[\Phi]$ depends on the system size in relation to the length scales determined by the system parameters. At $\mu = 0$ the p-wave superconductor lies within its topological phase, with corresponding localized MFs emerging at its endpoints. Taking again ℓ_M as a reference length scale, when $\ell \lesssim \ell_M$, the two MFs are hybridized into a Dirac mode Γ. As a result, the MFs have no significant effects on the current, which is 4π periodic, consistently with the expected behavior of the system as a mesoscopic normal ring [22]. On increasing ℓ, when $\ell > \ell_M$, the hybridization between the MFs becomes negligible and, accordingly, in the absence of fermion parity conservation, $I[\Phi]$ becomes 2π periodic, with jumps at $\Phi = \pi + 2\pi k$. In addition to the periodicity, also the shape of $I[\Phi]$ depends on ℓ. This is due to the
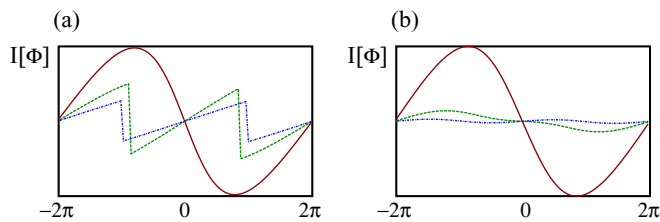

FIG. 10. Plot of $I[\Phi]$ vs Φ for a hybrid normal-superconducting ring. (a) Plot of $I[\Phi]$ vs Φ for a hybrid normal-p-wave superconducting ring for $w_1 = w_2 = 1$, $\Delta = 0.2$, $\tau = 0.5$, $\mu = 0$, which corresponds to $\ell_M \approx 6$, $\xi_{K,M} \approx 16$, for $\ell_S = \ell_N = 4$ (solid red curve), $\ell_S = \ell_N = 16$ (dashed green curve), $\ell_S = \ell_N = 40$ (dot-dashed blue curve). The crossover to a sawtooth behavior is evident for $\ell = 40$. (b) Plot of $I[\Phi]$ vs Φ for a hybrid normal-s-wave superconducting ring for $w_1 = w_2 = 1$, $\Delta = 0.2$, $\tau = 0.5$, for $\ell_S = \ell_N = 4$ (solid red curve), $\ell_S = \ell_N = 16$ (dashed green curve), $\ell_S = \ell_N = 40$ (dot-dashed blue curve). There is no crossover in the functional form of $I[\Phi]$, but a mere scaling of $I[\Phi]$ that is $\sim \ell_N^{-1}$.
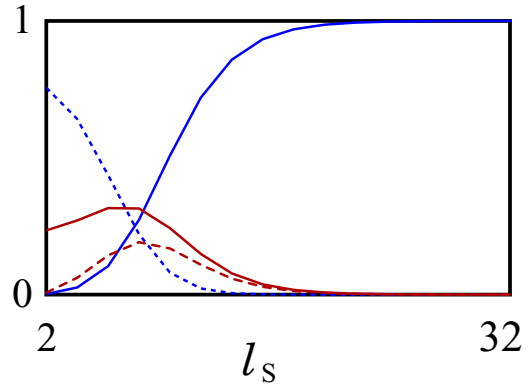

FIG. 11. Plot of the normal and Andreev reflection coefficients at the SN interface and of the normal transmission and CAR coefficients for the p-wave superconductor-normal hybrid ring discussed in Sec. IV B as a function of ℓ_S. To generate the plot we have chosen the system's parameters so that $w_1 = w_2 = 1$, $\Delta = 0.2$, $\tau = 0.5$, which corresponds to $\ell_M \approx 6$. The various curves correspond to the coefficients as: Full blue curve: Andreev reflection coefficient at the SN interface; dashed blue curve: normal reflection coefficient at the SN interface; full red curve: normal transmission across the superconducting region; and dashed red curve: crossed Andreev reflection across the superconducting region. Apparently, for $\ell_S > \ell_M$, all the processes are suppressed, except the Andreev reflection at the SN interface, with the corresponding coefficient saturating to 1.

Kondo-like hybridization between the MFs and the excitation modes within the normal region of the ring, which takes place when $\ell \gtrsim \xi_{K,M}$, with the Kondo-Majorana hybridization (KMH) length $\xi_{K,M} \sim [(2w)^2/\tau^2]$ [44]. At the onset of KMH, $I[\Phi]$ is expected to cross from a discontinuous sinusoidal dependence on Φ to a sawtoothlike shape [44]. Physically, this can be understood by recalling that, as ℓ becomes large, the systematic cancellation of contributions from high-energy states makes only low-energy states in the normal region next to the Fermi level contribute to $I[\Phi]$. The physical processes at the SN interfaces that determine these states can be inferred from Fig. 11, where, as a function of ℓ_S, we plot the scattering coefficients across the superconducting regions corresponding to normal reflection at the SN interfaces and to normal transmission across the superconducting region, as well as the coefficients corresponding to Andreev reflection (AR) at the interfaces and to "crossed Andreev reflection" (CAR) across the superconducting region [41,45]. As it clearly appears from Fig. 11, as soon as $\ell_S > \ell_M$, all the coefficients drop to 0 but the one corresponding to AR, which saturates to 1. This evidences that, as $\ell > \ell_S$, AR is the only physical process that takes place at low energy, which implies the sawtooth behavior in $I[\Phi]$ evidenced in Fig. 10(a). By comparison, in Fig. 10(b) we plot $I[\Phi]$ vs Φ for the same values of the various parameters as in Fig. 10(a), but for an s-wave superconductor. Here we see that, on increasing ℓ, the current still shows the crossover from a 4π-periodic curve to a 2π-periodic curve, but that the absence of low-energy Majorana modes eventually hybridizing with the modes in the normal region as $\ell \gtrsim \xi_{K,M}$ yields no crossover in the functional form of $I[\Phi]$ from a sinusoidal to a sawtooth behavior. The only relevant additional feature that takes place on varying ℓ is, indeed, the expected scaling of $I[\Phi] \sim \ell^{-1}$
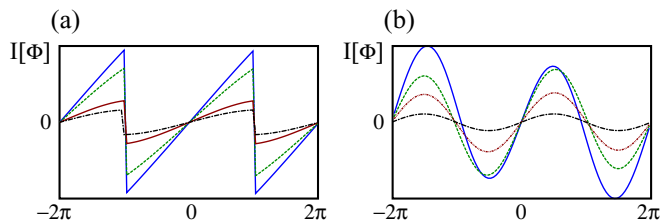
(a)

(b)

FIG. 12. Plot of $I[\Phi]$ vs Φ for a hybrid normal-superconducting ring. (a) Plot of $I[\Phi]$ vs Φ for a hybrid normal-p-wave superconducting ring for $w_1 = w_2 = 1$, $\Delta = 0.2$, $\tau = 0.5$, $\mu_N = 0$, which corresponds $\xi_{K,M} \approx 16$, $\ell_S = \ell_N = 40$ and $\mu_S/w = 0.0$ (solid blue curve), $\mu_S/w = 1.5$ (dashed green curve), $\mu_S/w = 1.9$ (dot-dashed red curve), and $\mu_S/w = 1.95$ (dot-dot-dashed black curve). (b) Same as in (a), but for a hybrid normal-s-wave superconducting ring for $w_1 = w_2 = 1$, $\Delta = 0.2$, $\tau = 0.5$, $\mu_N = 0$, $\ell_S = \ell_N = 40$ and $\mu_S/w = 0.0$ (solid blue curve), $\mu_S/w = 1.0$ (dashed green curve), $\mu_S/w = 1.5$ (dot-dashed red curve), and $\mu_S/w = 1.9$ (dot-dot-dashed black curve). (a) A clear smoothing of the sawtooth dependence of $I[\Phi]$ on Φ towards a sinusoidal plot as μ_S/w increases towards the critical value $\mu_S/w = 2$, at which Majorana fermions disappear.

(see discussion in the next section). Thus, the crossover in the functional form of $I[\Phi]$ can actually be regarded as a direct evidence for the existence of low-energy Majorana modes at the endpoints of the topological superconductor in the p-wave hybrid ring.

To further substantiate the above picture, in Fig. 12(a) we again plot $I[\Phi]$ vs Φ for the system parameters numerically set as discussed in the caption. In drawing Fig. 12, we hold $\ell_N = \ell_S$ fixed at 40 (with Δ and w chosen so that $\ell_M \sim 6$), as well as the chemical potential within the normal region $\mu_N = 0$. At variance we vary the chemical potential within the superconducting region μ_S starting from $\mu_S = 0$ till $\mu_S/w \sim 1.95$ (after which the loss of numerical precision appears not to give us reliable results). As highlighted by Kitaev [20], as $\mu_S/w = 2$ the p-wave superconductor undergoes a (topological) quantum phase transition, characterized by the disappearance (for $\mu_S/w > 2$) of the localized MFs at the endpoints of the superconductor. On approaching the phase transition from within the topological region, the closer the system is to the quantum critical point, the larger is the effective ℓ_M. While the actual numerical estimate of ℓ_M as a function of, e.g., μ_S/w at fixed Δ can in principle be provided from Eq. (A5) of the Appendix, here we just focus on the consistency of our exact results with the expectation one gets from the above discussion. In fact, the estimated KMH length for the system used to derive $I[\Phi]$ in Fig. 12(a) is $\xi_{K,M} \approx 16$ [see the discussion in the caption of Fig. 10(a), which is drawn at the same values of w and τ]. In Fig. 12(a) we plot $I[\Phi]$ for $\ell_S = \ell_N = 40$, we see full KMH in the normal region for $\mu_N = 0$, as evidenced by the sawtooth behavior of the current and by the corresponding 2π periodicity in Φ. On increasing μ_S towards the critical value corresponding to the topological quantum phase transition, the nonnegligible hybridization between the MFs across the superconducting region is expected to compete with KMH and eventually to suppress it (in fact, this can be regarded as a "Majorana

analog" of the competition between Kondo effect and RKKY interaction in the two-impurity Kondo model [46–49], just as the KMH can be regarded as the Majorana analog of the onset of the Kondo cloud in a Kondo system [44]). Consistently with the expectation, we see that, on increasing μ_S, the sawtooth is smoothed (with a sizable reduction in the critical current) and clearly evolves back towards a restoration of the 4π periodicity that characterizes the regime $\ell_S \leqslant \ell_M$ (see discussion above). For comparison, in Fig. 12(b) we draw similar plots generated in the s-wave case. No particular changes in the functional form of the current appear, except the reduction in the value of the current at a given Φ. In our view, this result does actually enforce the reliability of a persistent current measurement as a tool to detect the presence of MFs at the endpoints of a p-wave superconductor in the topological phase.

It is important to stress once more that, while our approach allowed for readily studying the additional consequences of KMH in the case of a hybrid ring with an extended normal region, due to the increasing complexity of the system, this would be hardly doable within an alternative approach, without resorting to some ad hoc approximations and possibly washing out some relevant physical effects. This enforces once more the importance of having an exact analytical formula that applies independently of the specific values of the system parameters. Besides the possibility of exactly computing the current in a number of different physical systems by simply evaluating the integral in Eq. (13) for different values of Φ, our approach also provide a remarkable tool to write, for large enough systems, $I[\Phi]$ in a power series of the inverse system size which, as we are going to discuss in the following, greatly simplifies the various calculations, by even providing explicit analytic results for the current, in some simple cases.

V. THE LARGE-RING LIMIT

As the ring size goes large, one may recast the integral formula for $I[\Phi]$, Eq. (13), in an expansion in inverse powers of the length that gets large. As we discuss in the following, this leads to a number of simplifications in the calculation of the current, similar to the ones implemented in Refs. [35,38], even leading, in some cases, to a closed-form analytic formula for $I[\Phi]$ vs Φ at given system parameters. In the following, we discuss a few examples of calculation of the persistent current in the large-size limit, also showing how a number of known results can be easily recovered within our formalism, once the appropriate limit is taken.

A. The limit of long superconducting region

The limit of long superconducting region is defined by sending $\ell_2 \to \infty$ in the system described by the model Hamiltonian in Eq. (14) (p-wave case), or by the Hamiltonian in Eq. (33) (s-wave case), after setting $\Delta_1 = 0$, so that region 1 is normal, and by keeping ℓ_1 finite. In this limit one expects to recover the results for a the Josephson current across an SNS-hybrid junction. To show that this is, in fact, the case, we start by rewriting $\det\{\mathcal{M}_{p\text{-wave}}[E;\Phi;\ell_1;\ell_2] - \mathbf{I}\}$ as

$$\det\{\mathcal{M}_{p\text{-wave}}[E;\Phi;\ell_1;\ell_2] - \mathbf{I}\}$$
$$= c \det\{\mathbf{T}_2^{-1}(E;\ell_2) - [\Upsilon^{(2)}(E)]^{-1}\Sigma_2^{-1}[\Phi]\Omega_1[\Phi]$$

$$\times [\Upsilon^{(1)}(E)]\mathbf{T}_1(E;\ell_1)[\Upsilon^{(1)}(E)]^{-1}\Sigma_1^{-1}[\Phi]$$

$$\times \Omega_2[\Phi][\Upsilon^{(2)}(E)], \tag{44}$$

with c being an overall factor independent of Φ and, similarly, by rewriting $\det\{\mathcal{M}_{s\text{-wave}}[E;\Phi;\ell_1;\ell_2] - \mathbf{I}\}$ as

$$\det\{\mathcal{M}_{s\text{-wave}}[E;\Phi;\ell_1;\ell_2] - \mathbf{I}\}$$
$$= c'\det\{\mathbf{T}_2^{-1}(E;\ell_2) - [\tilde{\Upsilon}^{(2)}(E)]^{-1}\tilde{\Sigma}_2^{-1}[\Phi]\tilde{\Omega}_1[\Phi]$$
$$\times [\tilde{\Upsilon}^{(1)}(E)]\mathbf{T}_1(E;\ell_1)[\tilde{\Upsilon}^{(1)}(E)]^{-1}\tilde{\Sigma}_1^{-1}[\Phi]$$
$$\times \tilde{\Omega}_2[\Phi][\tilde{\Upsilon}^{(2)}(E)]\}, \tag{45}$$

with, again, c' being a constant independent of Φ. As a next step, we define the matrix $\mathbf{M}_p$ as

$$\mathbf{M}_p = [\Upsilon^{(2)}(E)]^{-1}\Sigma_2^{-1}[\Phi]\Omega_1[\Phi][\Upsilon^{(1)}(E)]\mathbf{T}_1(E;\ell_1)$$
$$\cdot[\Upsilon^{(1)}(E)]^{-1}\Sigma_1^{-1}[\Phi]\Omega_2[\Phi][\Upsilon^{(2)}(E)], \tag{46}$$

for the p-wave hybrid ring, and

$$\mathbf{M}_s = [\tilde{\Upsilon}^{(2)}(E)]^{-1}\tilde{\Sigma}_2^{-1}[\Phi]\tilde{\Omega}_1[\Phi][\tilde{\Upsilon}^{(1)}(E)]\mathbf{T}_1(E;\ell_1)$$
$$\times [\tilde{\Upsilon}^{(1)}(E)]^{-1}\tilde{\Sigma}_1^{-1}[\Phi]\tilde{\Omega}_2[\Phi][\tilde{\Upsilon}^{(2)}(E)], \tag{47}$$

for the s-wave hybrid ring. From Eqs. (46) and (47) we see that the current in the p-wave and the s-wave hybrid ring $I_{p,s}[\Phi]$ can, respectively, be written as

$$I_{p,s}[\Phi] = -\frac{1}{2\pi i}\int_\Gamma dE\, \partial_\Phi \ln[\Psi_{p,s}[E;\Phi]]$$
$$= -\frac{1}{4\pi i}\int_\Gamma dE\, \partial_\Phi\{\ln\det[\mathbf{T}_2^{-1}(\epsilon;\ell_2) - \mathbf{M}_{p,s}]$$
$$- \{\ln\det[\mathbf{T}_2^{-1}(\epsilon;\ell_2) - \mathbf{M}_{p,s}]\}^*\}, \tag{48}$$

where we have used the reality of the persistent current to go through the last step in Eq. (48). In order to systematically take the $\ell_2 \to \infty$-limit, we recall that one has eventually to deform the integrals over Γ in Eq. (48) into integrals over the imaginary axis, which corresponds to $E \to i\omega$. Along the imaginary axis, from the dispersion relations for particlelike and holelike excitations within the superconducting region, one obtains that the corresponding momenta are defined by

$$\cos[k_p^{(2)}] = -\frac{\mu_2 w_2}{2(w_2^2 - \Delta_2^2)} - \frac{i}{2}\sqrt{\frac{\omega^2 + \Delta_w^2}{w_2^2 - \Delta_2^2}},$$
$$\cos[k_h^{(2)}] = -\frac{\mu_2 w_2}{2(w_2^2 - \Delta_2^2)} + \frac{i}{2}\sqrt{\frac{\omega^2 + \Delta_w^2}{w_2^2 - \Delta_2^2}}, \tag{49}$$

in the p-wave case, and

$$\cos[k_p^{(2)}] = -\frac{\mu_2}{2w_2} - \frac{i}{2}\sqrt{\frac{\omega^2 + \Delta_2^2}{w_2^2}},$$
$$\cos[k_h^{(2)}] = -\frac{\mu_2}{2w_2} + \frac{i}{2}\sqrt{\frac{\omega^2 + \Delta_2^2}{w_2^2}}, \tag{50}$$

in the s-wave case. To solve Eqs. (49) we therefore set

$$k_p^{(2)} = \frac{\pi}{2} + q_p, \quad k_h^{(2)} = \frac{\pi}{2} + q_p^*, \tag{51}$$

with

$$\sin[q_p] = \frac{\mu_2 w_2}{2(w_2^2 - \Delta_2^2)} + \frac{i}{2}\sqrt{\frac{\omega^2 + \Delta_w^2}{w_2^2 - \Delta_2^2}}, \tag{52}$$

while to solve Eqs. (50) we set

$$k_p^{(2)} = \frac{\pi}{2} + q_s, \quad k_h^{(2)} = \frac{\pi}{2} + q_s^*, \tag{53}$$

with

$$\sin[q_s] = \frac{\mu_2}{2w_2} + \frac{i}{2}\sqrt{\frac{\omega^2 + \Delta_2^2}{w_2^2}}. \tag{54}$$

From the explicit formula for $\mathbf{T}_{2;(p,s)}^{-1}(E \to i\omega; \ell_2)$ along the imaginary axis in the p-wave and in the s-wave case, respectively given by

$$\mathbf{T}_{2;(p,s)}^{-1}(E \to i\omega; \ell_2)$$
$$= \begin{bmatrix} i^{-\ell_2}e^{-iq_{p,s}^{(2)}\ell_2} & 0 & 0 & 0 \\ 0 & i^{\ell_2}e^{iq_{p,s}^{(2)}\ell_2} & 0 & 0 \\ 0 & 0 & i^{\ell_2}e^{i[q_{p,s}^{(2)}]^*\ell_2} & 0 \\ 0 & 0 & 0 & i^{-\ell_2}e^{-i[q_{p,s}^{(2)}]^*\ell_2} \end{bmatrix}, \tag{55}$$

we may readily compute the integrals in Eq. (48) in the limit $\ell_2 \to \infty$, obtaining

$$I_{p,s}[\Phi] = \frac{1}{2\pi}\int_{-\infty}^{\infty} d\omega\, \partial_\Phi \ln \mathcal{G}_{p,s}(E \to i\omega), \tag{56}$$

with $\mathcal{G}_{p,s}(E) = \mathbf{M}_{(p,s);(2,2)}(E)\mathbf{M}_{(p,s);(4,4)}(E) - \mathbf{M}_{(p,s);(2,4)}(E)\mathbf{M}_{(p,s);(4,2)}(E)$ and assuming (as done in Refs. [35,38]) that

(1) All the poles of $\mathcal{G}(E)$ lie over the real axis.

(2) $\mathcal{G}(E)$ is real if E lies over the real axis (and does not coincide with a pole of $\mathcal{G}$).

Equation (56) yields the dc-Josephson current in the infinite-ℓ_2 limit, in which the ring can be regarded as an idealized model for an SNS junction. In the specific case of s-wave superconductors, Eq. (52) has been derived in Ref. [35] for a single-channel junction starting from the S-matrix approach to effectively one-dimensional SNS junctions [32], and generalized in Ref. [38] to a multichannel junction. In fact, a comparison between Eq. (56) and Eqs. (7) and (9) of Ref. [35] also clarifies the identification between $\mathbf{M}_{p,s}$ in Eqs. (46) and (47) and the transfer matrix for the whole SNS junction, as introduced and discussed in Ref. [35] for the s-wave case. After resorting to the effective SNS-junction model, at a second stage one may implement the technique developed in Refs. [35,38] to write $I[\Phi]$ in a systematic expansion in inverse powers of ℓ_1. Basically, one considers that because one has

$$\mathbf{T}_1(E \to i\omega; \ell_2)$$
$$= \begin{bmatrix} i^{\ell_1}e^{iq_n^{(1)}\ell_1} & 0 & 0 & 0 \\ 0 & i^{-\ell_1}e^{-iq_n^{(1)}\ell_1} & 0 & 0 \\ 0 & 0 & i^{-\ell_1}e^{-i[q_n^{(1)}]^*\ell_1} & 0 \\ 0 & 0 & 0 & i^{\ell_1}e^{i[q_n^{(1)}]^*\ell_1} \end{bmatrix}, \tag{57}$$

with

$$\sin\left[q_n^{(1)}\right] = \frac{\mu_1}{2w_1} + \frac{i}{2}\frac{\omega}{w_1}, \tag{58}$$

then, only low-$|\omega|$ regions do effectively contribute to the integral in Eq. (56). As a result, one may first of all approximate $q_n^{(1)} \approx \bar{q} + i\sigma(\omega)$, with

$$\sin(\bar{q}) = \frac{\mu_1}{2w_1},$$

$$\sigma(\omega) = \frac{\omega}{2w_1\cos(\bar{q})}, \tag{59}$$

then, in integrating Eq. (56), one may rescale $\omega \to \omega\ell_1$ and eventually set the rescaled ω at 0 in all the contributions to the argument of the integral in which ω appears divided by ℓ_1 as ω/ℓ_1. Going along this procedure, one may compute the leading contribution to the current $[O(\ell_1^{-1})]$ by trading the original model Hamiltonian for a reduced boundary model, such as the one presented in Ref. [31] for the s-wave superconductors and the one used in Ref. [44] for the p-wave superconductor, which allows for recovering simple, closed-form analytical formulas for $I[\Phi]$.

B. The limit of long normal region

We now discuss the complementary limit of a long normal region, with ℓ_S less than, or comparable to, the coherence length of the superconducting region ξ_0. We first discuss the general formula and then consider the case of a hybrid s-wave superconducting ring as a specific example. In order to address the large-ℓ_N limit, let us first of all rewrite $\det\{\mathcal{M}_{p\text{-wave }(s\text{-wave})}[E; \Phi; \ell_1; \ell_2] - \mathbf{I}\}$ as

$$\det\{\mathcal{M}_{p\text{-wave }(s\text{-wave})}[E; \Phi; \ell_1; \ell_2] - \mathbf{I}\}$$
$$= c_{p,s}\det\{\mathbf{T}_1(E; \ell_1) - \mathbf{K}_{p,s}[E; \Phi; \ell_2]\}, \tag{60}$$

with $c_{p,s}$ being constants independent of Φ, and

$$\mathbf{K}_p[E; \Phi; \ell_2] = [\Upsilon^{(1)}(E)]^{-1}\Omega_1^{-1}[\Phi]\Sigma_2[\Phi][\Upsilon^{(2)}(E)]$$
$$\times \mathbf{T}_2^{-1}(E; \ell_2)[\Upsilon^{(2)}(E)]^{-1}\Omega_2^{-1}[\Phi]$$
$$\times \Sigma_1[\Phi][\Upsilon^{(1)}(E)],$$

$$\mathbf{K}_s[E; \Phi; \ell_2] = [\tilde{\Upsilon}^{(1)}(E)]^{-1}\tilde{\Omega}_1^{-1}[\Phi]\tilde{\Sigma}_2[\Phi][\tilde{\Upsilon}^{(2)}(E)]$$
$$\times \mathbf{T}_2^{-1}(E; \ell_2)[\tilde{\Upsilon}^{(2)}(E)]^{-1}\tilde{\Omega}_2^{-1}[\Phi]$$
$$\times \tilde{\Sigma}_1[\Phi][\tilde{\Upsilon}^{(1)}(E)]. \tag{61}$$

Equations (61) correspond to the standard identification we have employed so far, that is, region 1 has to be identified with the normal region and region 2 with the (either p-wave, or s-wave) superconducting region. Therefore, $\ell_1 = \ell_N$. Now, in order to recover the large-ℓ_N limit, we strictly follow the derivation of Refs. [35,38], that is, once we have deformed the integration path to the imaginary axis, we assume that only low-ω $(= -iE)$ regions do effectively contribute the integral in Eq. (13). This allows us first of all to approximate the inverse dispersion relation within the normal region as

$$k_{p,h} \approx k_F \pm i\lambda(\omega), \tag{62}$$

with $-2w_1\cos(k_F) = \mu_1$ and $\lambda(\omega) = \frac{\omega}{2w\sin(k_F)}$. On substituting Eqs. (62) into Eqs. (61), we may eventually rewrite Eq. (13) as

$$I_{p,s}[\Phi] = -\frac{2ew_1\sin(k_F)}{2\pi\ell_1}\partial_\Phi\int_0^\infty\frac{dz}{z}\ln\{\Xi_{p,s}[z; \Phi; \ell_2]\}, \tag{63}$$

with

$$\Xi_{p,s}[z; \Phi; \ell_2] = \det\left\{\begin{bmatrix} z & 0 & 0 & 0 \\ 0 & z^{-1} & 0 & 0 \\ 0 & 0 & z & 0 \\ 0 & 0 & 0 & z^{-1} \end{bmatrix}\right.$$
$$-\begin{bmatrix} e^{-ik_F\ell_1} & 0 & 0 & 0 \\ 0 & e^{ik_F\ell_1} & 0 & 0 \\ 0 & 0 & e^{ik_F\ell_1} & 0 \\ 0 & 0 & 0 & e^{-ik_F\ell_1} \end{bmatrix}$$
$$\left.\times \mathbf{K}_{p,s}[E = 0; \Phi; \ell_2]\right\}. \tag{64}$$

To illustrate the effectiveness of our simplified Eqs. (63) and (64) we now discuss the application to the case of a hybrid s-wave superconducting ring. For simplicity we make the assumptions $w_1 = w_2 \equiv w$ and $\mu_1 = 0$. As a result, using Eqs. (63) and (64), we obtain the simplified expression for the current

$$I[\Phi] = -\frac{2ew_1\sin(k_F)}{2\pi\ell_1}\partial_\Phi\int_0^\infty\frac{dz}{z}\left\{\frac{\partial_\Phi a[\Phi; \ell_1](z^3 + z) + \partial_\Phi b[\Phi; \ell_2]z^2}{z^4 + 1 + a[\Phi; \ell_2](z^3 + z) + b[\Phi; \ell_2]z^2}\right\}, \tag{65}$$

with $a[\Phi; \ell_2], b[\Phi; \ell_2]$ being long, though straightforward to derive, functions of the matrix elements of $\mathbf{K}_s[E = 0; \Phi; \ell_2]$. Eventually, by means of simple manipulations Eq. (65) can be expressed as a closed-form formula only of the four roots $z_j[\Phi; \ell_2]$ $(j = 1, \ldots, 4)$ of the polynomial equation $z^4 + 1 + a[\Phi; \ell_2](z^3 + z) + b[\Phi; \ell_2]z^2 = 0$, which take the generic form

$$z_j[\Phi; \ell_2] = -\frac{a[\Phi; \ell_2]}{4} + u_j\frac{\sqrt{8 + a^2[\Phi; \ell_2] - 4b[\Phi; \ell_2]}}{4}$$
$$+ v_j\frac{1}{2}\sqrt{-2 + \frac{a^2[\Phi; \ell_2]}{4} - b[\Phi; \ell_2] + u_j\frac{a^3[\Phi; \ell_2] + 8a[\Phi; \ell_2] - 4a[\Phi; \ell_2]b[\Phi; \ell_2]}{2\sqrt{8 - a^2[\Phi; \ell_2] - 4b[\Phi; \ell_2]}b[\Phi; \ell_2]}}, \tag{66}$$

with $u_j, v_j = \pm 1$. Taking into account that $\prod_{j=1}^4 z_j[\Phi; \ell_2] = 1$, one eventually obtains from Eq. (65)

$$I[\Phi] = -\frac{2ew_1 \sin(k_F)}{4\pi \ell_1} \partial_\Phi \left\{ \sum_{j=1}^4 \ln^2[z_j[\Phi; \ell_2]] \right\}. \tag{67}$$

Just as in the case of a long SNS junction [35,38], Eq. (67) only involves data at the Fermi level. This is an additional example of the remarkable simplifications to which our approach leads, in the large ring limit.

VI. FINITE-TEMPERATURE RESULTS

It is not difficult to generalize our derivation to a system at temperature T finite, though much lower than the critical temperature for the superconducting part of the ring. In fact, at finite T, Eq. (13) generalizes to Eq. (1), with

$$F[\Phi; T] = \sum_E E f(E), \tag{68}$$

and $f(E) = [1 + e^{E/T}]^{-1}$ being the Fermi distribution function (having set the Boltzmann constant $k = 1$). Now, the integration path Γ in Eq. (11) must be replaced with the integration path $\tilde{\Gamma}$ obtained as the union of small circles Γ_n, each one surrounding once one, and only one, energy eigenvalue. As illustrated in Fig. 13, $\tilde{\Gamma}$ can be deformed to a path obtained as the union of small circles, each one surrounding once one, and only one, pole of the Fermi function, that is, a fermionic Matsubara frequency times the imaginary unit i, $i\omega_m = 2\pi T i(m + \frac{1}{2})$. As a result, the finite-T current can be presented as

$$I[\Phi; T] = -eT \sum_{\omega_m} \partial_\Phi \{\det[\mathcal{M}[i\omega_m; \Phi] - \mathbf{I}]\}, \tag{69}$$

that is the appropriate generalization of Eq. (13) to the finite-T case.

VII. DISCUSSION AND CONCLUSIONS

In this paper we have presented a technique to exactly compute the zero-temperature persistent current across an HR pierced by a magnetic flux Φ as a single integral of a known function of the system's parameters. Our approach
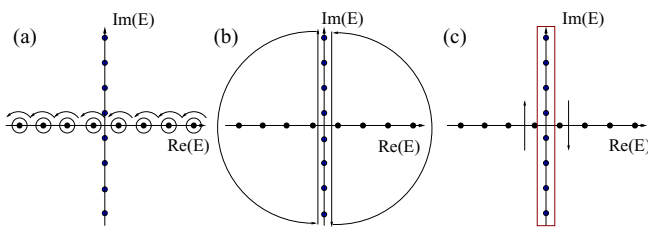

FIG. 13. Sequence of deformations in the integration path $\tilde{\Gamma}$ eventually allowing us to express $I[\Phi; T]$ as a sum over the fermionic Matsubara frequencies $\omega_m = 2\pi T(m + \frac{1}{2})$: (a) The path $\tilde{\Gamma}$ obtained as the union of small circles, each one surrounding one, and only one, energy eigenvalue. (b) The integral over $\tilde{\Gamma}$ can be deformed to an integral over the union of the two closed path run through counterclockwise. (c) The integral over the two closed path in (b) is equal to the integral over a closed path surrounding the poles of the Fermi function ($i\omega_m$, displayed as blue full circles in the figure), run through clockwise. The corresponding overall sign is eventually canceled by the -1 at the residue of the Fermi function at $i\omega_m$.

makes use of the properties of the transfer matrix of the ring, which allows us to circumvent technical difficulties associated with the secular equation for the energy eigenvalues of the system. A straightforward generalization of the zero-temperature formalism allows us to also compute the current in a ring at a temperature T finite, though much lower than the superconducting gap. While in general one may readily numerically compute the integral/sum yielding the current at a given value of the flux Φ, a remarkable simplification takes place in the limit of a large ring size, where resorting to a systematic expansion in inverse powers of the ring length allows for deriving the current in analytic closed-form formulas, applicable to a number of cases of physical interest.

As an example of application of our technique, we exactly compute the persistent current through a p-wave superconducting-normal ring as well as in an s-wave superconducting-normal ring. As a side result, we recover at once the crossover in the current periodicity, the effects of localized MFs in the p-wave case (including the signature of the topological phase transition), the large-size limit, etc., which were previously approximatively derived by means of various approximation schemes, different from case to case [28,29,35,38].

Throughout all the paper, we grounded our approach on a description of the ring in terms of a noninteracting lattice model Hamiltonian for the normal part of the ring, in terms of a non-self-consistent mean field Hamiltonian for the superconducting part. The system is assumed to be "clean," that is, no disorder effects are taken into account and no interaction between the electrons is assumed. As a further development of our research, we plan to generalize our approach, so to introduce the effect of disorder by means of a pertinently chosen impurity potential and by eventually ensemble averaging over the disorder realization [50,51], and the effect of the interaction, by adopting a pertinently adapted version of the fermion renormalization group approach introduced in Refs. [52–54] for weakly interacting systems and generalized in Ref. [55] to the strongly interacting case. This might potentially provide an useful method to also spell out the dynamics of fractionalized excitations in correlated systems [56–58]. Moreover, by simply sending to infinity the length of the superconducting part of the ring, our approach provides an exact formula for the Josephson current across an SNS junction, which can be readily applied to cases hard to deal with using alternative techniques, such as in the case of the anomalous Josephson effect in nanowires [59–61].

These, and other potentially interesting generalizations of our approach, do actually lie beyond the range of this paper, and we plan to address them as a future development of our work.

APPENDIX: EXACT WAVE FUNCTIONS FOR SUBGAP STATES AT A FINITE-LENGTH KITAEV CHAIN

In this Appendix we discuss in detail the derivation of the exact wave function of subgap states in an open Kitaev chain, of finite length ℓ_S. To do so, we employ a simplified and pertinently adapted version of the solution of the Kitaev model with open boundary conditions [62,63]. While for finite-ℓ_S we find a single Dirac fermion level, which can be either empty or filled with a corresponding finite energy gap E_M, as $\ell_S \to \infty$, the states become degenerate in energy at the Fermi level, and appropriate linear combinations of the corresponding wave functions become localized at the two endpoints of the chain, eventually corresponding to the two zero-energy Majorana solutions of Kitaev's model [20]. The starting point is the dispersion relation in Eqs. (23) which, for subgap solutions ($|E| < \Delta_w$) yields the allowed values of the (complex conjugate) particle and hole momenta defined by

$$\cos(k_p) = -\frac{w\mu}{2(w^2 - \Delta^2)} - \frac{i}{2}\sqrt{\frac{\Delta_w^2 - E^2}{w^2 - \Delta^2}},$$

$$\cos(k_h) = -\frac{w\mu}{2(w^2 - \Delta^2)} + \frac{i}{2}\sqrt{\frac{\Delta_w^2 - E^2}{w^2 - \Delta^2}}. \quad \text{(A1)}$$

Equations (A1) are readily solved by setting $k_p = \pi - q_R + iq_I$ and $k_h = (k_p)^* = \pi - q_R - iq_I$, with

$$\cos(q_R)\cosh(q_I) = \frac{w\mu}{2(w^2 - \Delta^2)},$$

$$\sin(q_R)\sinh(q_I) = \frac{1}{2}\sqrt{\frac{\Delta_w^2 - E^2}{w^2 - \Delta^2}}. \quad \text{(A2)}$$

As a result, the general formula for a subgap solution will be given by

$$\begin{bmatrix} u_j \\ v_j \end{bmatrix} = (-1)^j \left\{ A_{(p,+)} \begin{bmatrix} u \\ v \end{bmatrix} e^{-iq_R j} e^{-q_I j} \right.$$

$$+ A_{(p,-)} \begin{bmatrix} u \\ -v \end{bmatrix} e^{iq_R j} e^{q_I j} + A_{(h,+)} \begin{bmatrix} u^* \\ v^* \end{bmatrix} e^{iq_R j} e^{-q_I j}$$

$$\left. + A_{(h,-)} \begin{bmatrix} u^* \\ -v^* \end{bmatrix} e^{-iq_R j} e^{q_I j} \right\}, \quad \text{(A3)}$$

with u, v solutions of the algebraic system

$$\{E + 2w\cos(k_p) + \mu\}u - 2i\Delta\sin(k_p)v = 0,$$

$$2i\Delta\sin(k_p)u + \{E - 2w\cos(k_p) - \mu\}v = 0. \quad \text{(A4)}$$

The actual energy eigenstates are determined as nontrivial solutions such as the one in Eq. (A3) satisfying the boundary conditions on the "ghost sites" given by $\begin{bmatrix} u_0 \\ v_0 \end{bmatrix} = \begin{bmatrix} u_{\ell+1} \\ v_{\ell+1} \end{bmatrix} = 0$. It is therefore straightforward to verify that this implies the secular equation for the energy eigenvalues given by

$$[\text{Im}\, m(uv^*)]^2 \sinh^2[q_I(\ell + 1)]$$

$$= [\text{Re}\, e(uv^*)]^2 \sin^2[q_R(\ell + 1)]. \quad \text{(A5)}$$

Equations (A3), (A4), and (A5) can be used to estimate the energy of the subgap levels and the corresponding wave function for any value of μ. Indeed, we use them to numerically estimate the energy gap and to accordingly infer the overlap scale between the localized MFs at given values of the system's parameters. Specifically, if one is only interested in the low-energy physics of a finite-size one-dimensional topological superconductor coupled to normal conductors at each of its endpoints, the whole topological superconductor can be traded for an effective Hamiltonian involving only the low-energy subgap degrees of freedom discussed above, with parameters effectively determined by the actual system parameters. To illustrate how the procedure works, let us focus onto the simple case $\mu = 0$, ℓ even. In this case, k_p and k_h are simply given by

$$k_p = \frac{\pi}{2} + i\lambda(E),$$

$$k_h = \frac{\pi}{2} - i\lambda(E), \quad \text{(A6)}$$

with

$$\sinh[\lambda(E)] = \frac{1}{2}\sqrt{\frac{4\Delta^2 - E^2}{w^2 - \Delta^2}}. \quad \text{(A7)}$$

As a result, Eq. (A3) can now be presented as

$$\begin{bmatrix} u_j \\ v_j \end{bmatrix} = A_{(p,+)} \begin{bmatrix} u \\ v \end{bmatrix} i^j e^{-\lambda(E)j} + A_{(p,-)} \begin{bmatrix} u \\ -v \end{bmatrix} i^{-j} e^{\lambda(E)j}$$

$$+ A_{(h,+)} \begin{bmatrix} u^* \\ v^* \end{bmatrix} i^{-j} e^{-\lambda(E)j} + A_{(h,-)} \begin{bmatrix} u^* \\ -v^* \end{bmatrix} i^j e^{\lambda(E)j}, \quad \text{(A8)}$$

with

$$\begin{bmatrix} u_p \\ v_p \end{bmatrix} = \frac{1}{\sqrt{2}} \begin{bmatrix} e^{\frac{i}{2}\text{sgn}(E)\vartheta} \\ i\,\text{sgn}(E)e^{-\frac{i}{2}\text{sgn}(E)\vartheta} \end{bmatrix},$$

$$\begin{bmatrix} u_h \\ v_h \end{bmatrix} = \frac{1}{\sqrt{2}} \begin{bmatrix} -i\,\text{sgn}(E)e^{-\frac{i}{2}\text{sgn}(E)\vartheta} \\ e^{\frac{i}{2}\text{sgn}(E)\vartheta} \end{bmatrix}, \quad \text{(A9)}$$

and

$$\vartheta = \text{atan}\left[\frac{2w\sinh[\lambda(E)]}{|E|}\right]. \quad \text{(A10)}$$

It is straightforward, though tedious, to show that the secular equation for the subgap energy eigenvalues is now given by

$$(\ell + 1)\lambda(E) = \pm \sinh^{-1}\left[\frac{2w}{E}\sinh[\lambda(E)]\right], \quad \text{(A11)}$$

which is solved by setting

$$|E| = \epsilon = 2\Delta\left[\frac{\cosh[\lambda(E)]}{\cosh[(\ell + 1)\lambda(E)]}\right] \approx 2\Delta e^{-\ell\lambda(E)}$$

$$\approx 2\Delta \exp\left\{-\ell\sinh^{-1}\left[\frac{\Delta}{\sqrt{w^2 - \Delta^2}}\right]\right\}. \quad \text{(A12)}$$

Therefore, from Eq. (A12), we readily estimate that the hybridization length scale between the MFs ℓ_M is given

by

$$\ell_M \sim \left\{ \sinh^{-1}\left[\frac{\Delta}{\sqrt{w^2 - \Delta^2}}\right] \right\}^{-1}. \tag{A13}$$

From Eq. (A3) we may therefore construct the wave functions corresponding to the positive- and to the negative-energy subgap solutions. As a result, one obtains for the positive subgap energy solution of the BdG equations

$$\begin{bmatrix} u_j \\ v_j \end{bmatrix}_+ = c\left\{ e^{\frac{\xi}{2}} \begin{bmatrix} e^{\frac{i}{2}\vartheta} \\ ie^{-\frac{i}{2}\vartheta} \end{bmatrix} i^j e^{-j\lambda(E)} + ie^{-\frac{\xi}{2}} \begin{bmatrix} e^{\frac{i}{2}\vartheta} \\ -ie^{-\frac{i}{2}\vartheta} \end{bmatrix} i^{-j} e^{j\lambda(E)} \right.$$
$$+ e^{\frac{\xi}{2}} \begin{bmatrix} -ie^{-\frac{i}{2}\vartheta} \\ -e^{\frac{i}{2}\vartheta} \end{bmatrix} i^{-j} e^{-j\lambda(E)}$$
$$\left. - ie^{-\frac{\xi}{2}} \begin{bmatrix} -ie^{-\frac{i}{2}\vartheta} \\ e^{\frac{i}{2}\vartheta} \end{bmatrix} i^j e^{j\lambda(E)} \right\}, \tag{A14}$$

with

$$c = \frac{1}{4}\sqrt{\frac{2\sinh[\lambda(E)]}{\sinh[\xi[E] - \lambda(E)]}}, \tag{A15}$$

and $\xi[E] = \sinh^{-1}\left[\frac{2w}{E}\sinh[\lambda(E)]\right]$. Similarly, one obtains for the negative-energy subgap solution of the BdG equations

$$\begin{bmatrix} u_j \\ v_j \end{bmatrix}_- = -c\left\{ e^{\frac{\xi}{2}} \begin{bmatrix} e^{-\frac{i}{2}\vartheta} \\ -ie^{\frac{i}{2}\vartheta} \end{bmatrix} i^j e^{-j\lambda(E)} - ie^{-\frac{\xi}{2}} \begin{bmatrix} e^{-\frac{i}{2}\vartheta} \\ ie^{\frac{i}{2}\vartheta} \end{bmatrix} i^{-j} e^{j\lambda(E)} \right.$$
$$\left. + e^{\frac{\xi}{2}} \begin{bmatrix} ie^{\frac{i}{2}\vartheta} \\ -e^{-\frac{i}{2}\vartheta} \end{bmatrix} i^{-j} e^{-j\lambda(E)} + ie^{-\frac{\xi}{2}} \begin{bmatrix} ie^{\frac{i}{2}\vartheta} \\ e^{-\frac{i}{2}\vartheta} \end{bmatrix} i^j e^{j\lambda(E)} \right\}. \tag{A16}$$

From Eqs. (A14) and (A16) we therefore find that the eigenmodes corresponding to the $\pm$ solutions are respectively given by

$$\Gamma_+ = \sum_{j=1}^{\ell}\{[u_j]_+^* c_j + [v_j]_+^* c_j^\dagger\},$$

$$\Gamma_- = \sum_{j=1}^{\ell}\{[u_j]_-^* c_j + [v_j]_-^* c_j^\dagger\}, \tag{A17}$$

which shows that, as expected, one recovers the relation

$$\Gamma_+ = \Gamma_-^\dagger \equiv \Gamma. \tag{A18}$$

On inverting Eqs. (A17) and truncating the mode expansion of the real space lattice operators by retaining low-energy modes only, we therefore get

$$c_j \approx [u_j]_+ \Gamma + [v_j]_+^* \Gamma^\dagger,$$
$$c_j^\dagger \approx [v_j]_+ \Gamma + [u_j]_+^* \Gamma^\dagger. \tag{A19}$$

Now, on calling $\{d_j, d_j^\dagger\}$ and ℓ_N the length of the normal part of the ring, the fermion operators on the normal side, one may rewrite the tunneling contribution to the Hamiltonian in Eq. (14) as

$$H_\tau = -\tau\left\{\left[c_1^\dagger d_{\ell_N} + d_1^\dagger c_{\ell_N}\right]e^{\frac{i}{4}\Phi} + \left[d_{\ell_N}^\dagger c_1 + c_\ell^\dagger d_1\right]e^{-\frac{i}{4}\Phi}\right\}. \tag{A20}$$

Using the truncated expansions in Eqs. (A19) and the explicit form of the wave functions evaluated at $j = 1, \ell$, one eventually approximates Eq. (A20) as

$$H_\tau = t_L\left\{\gamma_L\left[e^{\frac{i}{4}\Phi} d_{\ell_N} - e^{-\frac{i}{4}\Phi} d_{\ell_N}^\dagger\right]\right\}$$
$$+ it_R\{\gamma_R[e^{-\frac{i}{4}\Phi} d_1 + e^{\frac{i}{4}\Phi} d_1^\dagger]\}, \tag{A21}$$

with

$$\gamma_L = e^{-i\frac{\pi}{4}}\Gamma + e^{i\frac{\pi}{4}}\Gamma^\dagger,$$
$$\gamma_R = -i\{e^{-i\frac{\pi}{4}}\Gamma - e^{i\frac{\pi}{4}}\Gamma^\dagger\}. \tag{A22}$$

and $t_L = t_R = \Upsilon\tau$, with

$$u_{1,+} = -e^{-i\frac{\pi}{4}}\Upsilon,$$
$$v_{1,+} = -e^{-i\frac{\pi}{4}}\Upsilon,$$
$$u_{\ell,+} = -e^{-i\frac{\pi}{4}}\Upsilon,$$
$$v_{\ell,+} = e^{-i\frac{\pi}{4}}\Upsilon. \tag{A23}$$

Finally, to recover the energy bias between the Dirac modes, we add a term of the form

$$H_\Gamma = 2\epsilon\{2\Gamma^\dagger\Gamma - 1\} = -2\epsilon i\gamma_L\gamma_R. \tag{A24}$$

In general, t_L, t_R are smooth functions of μ. The dependence of ϵ on μ can be inferred by numerically solving Eq. (A5), as we did in the main text, to also derive the dependence of ℓ_M on the chemical potential.

[1] M. Thinkam, *Introduction to Superconductivity* (Dover, New York, 2004).

[2] Y. Imry, *Introduction to Mesoscopic Physics* (Oxford University Press, London, 2002).

[3] J. File and R. G. Mills, Phys. Rev. Lett. **10**, 93 (1963).

[4] M. Büttiker, Y. Imry, and M. Landauer, Phys. Lett. A **96**, 365 (1983).

[5] H. Bluhm, N. C. Koshnick, J. A. Bert, M. E. Huber, and K. A. Moler, Phys. Rev. Lett. **102**, 136802 (2009).

[6] A. C. Bleszynski-Jayich, W. E. Shanks, B. Peaudecerf, E. Ginossar, F. von Oppen, L. Glazman, and J. G. E. Harris, Science **326**, 272 (2009).

[7] H.-F. Cheung, Y. Gefen, E. K. Riedel, and W.-H. Shih, Phys. Rev. B **37**, 6050 (1988).

[8] G. Montambaux, H. Bouchiat, D. Sigeti, and R. Friesner, Phys. Rev. B **42**, 7647 (1990).

[9] D. Loss and P. Goldbart, Phys. Rev. B **43**, 13762 (1991).

[10] A. Müller-Groeling, H. A. Weidenmüller, and C. H. Lewenkopf, Europhys. Lett. **22**, 193 (1993).

[11] J. Splettstoesser, M. Governale, and U. Zülicke, Phys. Rev. B **68**, 165341 (2003).

[12] S. K. Maiti, Quantum Matter **3**, 413 (2014).

[13] D. Giuliano and P. Sodano, Nucl. Phys. B **770**, 332 (2007).

[14] A. Cirillo, M. Mancini, D. Giuliano, and P. Sodano, Nucl. Phys. B **852**, 235 (2011).

[15] D. Giuliano and P. Sodano, Europhys. Lett. **88**, 17012 (2009).

[16] D. Giuliano and P. Sodano, Nucl. Phys. B **837**, 153 (2010).

[17] F. V. M., *Physics of Quantum Rings* (Springer, Berlin, 2014).

[18] J. Cayssol, T. Kontos, and G. Montambaux, Phys. Rev. B **67**, 184508 (2003).

[19] M. Büttiker and T. M. Klapwijk, Phys. Rev. B **33**, 5114 (1986).

[20] A. Y. Kitaev, Phys. Usp. **44**, 131 (2001).

[21] R. M. Lutchyn, J. D. Sau, and S. Das Sarma, Phys. Rev. Lett. **105**, 077001 (2010).

[22] Y. Oreg, G. Refael, and F. von Oppen, Phys. Rev. Lett. **105**, 177002 (2010).

[23] V. Mourik, K. Zuo, S. M. Frolov, S. R. Plissard, E. P. A. M. Bakkers, and L. P. Kouwenhoven, Science **336**, 1003 (2012).

[24] J. Liu, A. C. Potter, K. T. Law, and P. A. Lee, Phys. Rev. Lett. **109**, 267002 (2012).

[25] E. Dumitrescu, B. Roberts, S. Tewari, J. D. Sau, and S. Das Sarma, Phys. Rev. B **91**, 094505 (2015).

[26] F. Dessotti, L. Ricco, Y. Marques, L. Guessi, M. Yoshida, M. Figueira, M. de Souza, P. Sodano, and A. Seridonio, Phys. Rev. B **94**, 125426 (2016).

[27] P. Lucignano, F. Tafuri, and A. Tagliacozzo, Phys. Rev. B **88**, 184512 (2013).

[28] P. Jacquod and M. Büttiker, Phys. Rev. B **88**, 241409 (2013).

[29] F. Pientka, A. Romito, M. Duckheim, Y. Oreg, and F. von Oppen, New J. Phys. **15**, 025001 (2013).

[30] G. E. Blonder, M. Tinkham, and T. M. Klapwijk, Phys. Rev. B **25**, 4515 (1982).

[31] I. Affleck, J.-S. Caux, and A. M. Zagoskin, Phys. Rev. B **62**, 1433 (2000).

[32] C. W. J. Beenakker, Phys. Rev. Lett. **67**, 3836 (1991).

[33] A. Furusaki and M. Tsukada, Solid State Commun. **78**, 299 (1991).

[34] C. W. J. Beenakker, *Three "Universal" Mesoscopic Josephson Effects* (Springer, Berlin, 1992), pp. 235–253.

[35] D. Giuliano and I. Affleck, J. Stat. Mech. (2013) P02034.

[36] P. Brouwer and C. Beenakker, Chaos Solitons Fractals **8**, 1249 (1997).

[37] C. W. J. Beenakker, D. I. Pikulin, T. Hyart, H. Schomerus, and J. P. Dahlhaus, Phys. Rev. Lett. **110**, 017003 (2013).

[38] D. Giuliano and I. Affleck, Phys. Rev. B **90**, 045133 (2014).

[39] P. A. Mello and N. Kumar, *Quantum Transport in Mesoscopic Systems: Complexity and Statistical Fluctuations, a Maximum-entropy Viewpoint* (Oxford University Press, London, 2004).

[40] X. Chen, Z.-Y. Deng, W. Lu, and S. C. Shen, Phys. Rev. B **61**, 2008 (2000).

[41] M. Lee, H. Khim, and M.-S. Choi, Phys. Rev. B **89**, 035309 (2014).

[42] K. A. Matveev, A. I. Larkin, and L. I. Glazman, Phys. Rev. Lett. **89**, 096802 (2002).

[43] D. I. Pikulin, Y. Komijani, and I. Affleck, Phys. Rev. B **93**, 205430 (2016).

[44] I. Affleck and D. Giuliano, J. Stat. Phys. **157**, 666 (2014).

[45] K. T. Law, P. A. Lee, and T. K. Ng, Phys. Rev. Lett. **103**, 237001 (2009).

[46] C. Jayaprakash, H. R. Krishna-murthy, and J. W. Wilkins, Phys. Rev. Lett. **47**, 737 (1981).

[47] B. A. Jones, C. M. Varma, and J. W. Wilkins, Phys. Rev. Lett. **61**, 125 (1988).

[48] I. Affleck and A. W. W. Ludwig, Phys. Rev. Lett. **68**, 1046 (1992).

[49] I. Affleck, A. W. W. Ludwig, and B. A. Jones, Phys. Rev. B **52**, 9528 (1995).

[50] G. Campagnano and Yu. V. Nazarov, Phys. Rev. B **74**, 125307 (2006).

[51] G. Campagnano, O. N. Jouravlev, Ya. M. Blanter, and Yu. V. Nazarov, Phys. Rev. B **69**, 235319 (2004).

[52] K. A. Matveev, D. Yue, and L. I. Glazman, Phys. Rev. Lett. **71**, 3351 (1993).

[53] D. Yue, L. I. Glazman, and K. A. Matveev, Phys. Rev. B **49**, 1966 (1994).

[54] S. Lal, S. Rao, and D. Sen, Phys. Rev. B **66**, 165327 (2002).

[55] D. Giuliano and A. Nava, Phys. Rev. B **92**, 125138 (2015).

[56] Z. Cai, C. Wu, and U. Schollwöck, Phys. Rev. B **85**, 075102 (2012).

[57] B. A. Bernevig, D. Giuliano, and R. B. Laughlin, Phys. Rev. Lett. **86**, 3392 (2001).

[58] B. A. Bernevig, D. Giuliano, and R. B. Laughlin, Phys. Rev. Lett. **87**, 177206 (2001).

[59] T. Yokoyama, M. Eto, and Y. V. Nazarov, J. Phys. Soc. Jpn. **82**, 054703 (2013).

[60] T. Yokoyama, M. Eto, and Y. V. Nazarov, Phys. Rev. B **89**, 195407 (2014).

[61] G. Campagnano, P. Lucignano, D. Giuliano, and A. Tagliacozzo, J. Phys.: Condens. Matter **27**, 205301 (2015).

[62] D. Giuliano, P. Sodano, A. Tagliacozzo, and A. Trombettoni, Nucl. Phys. B **909**, 135 (2016).

[63] M. Fagotti, J. Stat. Mech. (2016) 063105.